Journal of Geophysical Research: Space Physics

RESEARCH ARTICLE
10.1002/2017JA025046

Key Points:
- The study presents the results of a large HST campaign observing Jupiter's UV aurora, concurrently with the in situ exploration of its magnetosphere with Juno
- The study provides an original analysis method based on the definition of six morphological families tentatively associated with Jupiter's magnetospheric state
- This HST data set provides crucial synergistic measurements and additional opportunities to augment the Juno mission science return

Supporting Information:
- Supporting Information S1

Correspondence to:
D. Grodent,
d.grodent@uliege.be

Citation:
Grodent, D., Bonfond, B., Yao, Z., Gérard, J.-C., Radioti, A., Dumont, M., et al. (2018). Jupiter's aurora observed with HST during Juno orbits 3 to 7. *Journal of Geophysical Research: Space Physics*, *123*. https://doi.org/10.1002/2017JA025046

Received 24 NOV 2017
Accepted 9 MAR 2018
Accepted article online 12 MAR 2018

Jupiter's Aurora Observed With HST During Juno Orbits 3 to 7

Denis Grodent[1], B. Bonfond[1], Z. Yao[1], J.-C. Gérard[1], A. Radioti[1], M. Dumont[1], B. Palmaerts[1], A. Adriani[2], S. V. Badman[3], E. J. Bunce[4], J. T. Clarke[5], J. E. P. Connerney[6], G. R. Gladstone[7], T. Greathouse[7], T. Kimura[8], W. S. Kurth[9], B. H. Mauk[10], D. J. McComas[11], J. D. Nichols[4], G. S. Orton[12], L. Roth[13], J. Saur[14], and P. Valek[7,15]

[1]Laboratoire de Physique Atmosphérique et Planétaire, STAR Institute, Université de Liège, Liège, Belgium, [2]Istituto di Astrofisica e Planetologia Spaziali, INAF, Rome, Italy, [3]Physics Department, Lancaster University, Lancaster, UK, [4]Department of Physics and Astronomy, University of Leicester, Leicester, UK, [5]Center for Space Physics, Boston University, Boston, MA, USA, [6]Solar System Exploration Division, Planetary Magnetospheres Laboratory, NASA Goddard Space Flight Center, Greenbelt, MD, USA, [7]Space Science Department, Southwest Research Institute, San Antonio, TX, USA, [8]RIKEN, Wako, Japan, [9]Department of Physics and Astronomy, The University of Iowa, Iowa City, IA, USA, [10]Applied Physics Laboratory, The Johns Hopkins University, Laurel, MD, USA, [11]Department of Astrophysical Sciences, Princeton University, Princeton, NJ, USA, [12]Jet Propulsion Laboratory, California Institute of Technology, Pasadena, CA, USA, [13]School of Electrical Engineering, Royal Institute of Technology KTH, Stockholm, Sweden, [14]Institute of Geophysics and Meteorology, University of Cologne, Cologne, Germany, [15]Department of Physics and Astronomy, University of Texas at San Antonio, San Antonio, TX, USA

Abstract A large set of observations of Jupiter's ultraviolet aurora was collected with the Hubble Space Telescope concurrently with the NASA-Juno mission, during an eight-month period, from 30 November 2016 to 18 July 2017. These Hubble observations cover Juno orbits 3 to 7 during which Juno in situ and remote sensing instruments, as well as other observatories, obtained a wealth of unprecedented information on Jupiter's magnetosphere and the connection with its auroral ionosphere. Jupiter's ultraviolet aurora is known to vary rapidly, with timescales ranging from seconds to one Jovian rotation. The main objective of the present study is to provide a simplified description of the global ultraviolet auroral morphology that can be used for comparison with other quantities, such as those obtained with Juno. This represents an entirely new approach from which logical connections between different morphologies may be inferred. For that purpose, we define three auroral subregions in which we evaluate the auroral emitted power as a function of time. In parallel, we define six auroral morphology families that allow us to quantify the variations of the spatial distribution of the auroral emission. These variations are associated with changes in the state of the Jovian magnetosphere, possibly influenced by Io and the Io plasma torus and by the conditions prevailing in the upstream interplanetary medium. This study shows that the auroral morphology evolved differently during the five ~2 week periods bracketing the times of Juno perijove (PJ03 to PJ07), suggesting that during these periods, the Jovian magnetosphere adopted various states.

1. Introduction

The National Aeronautics and Space Administration (NASA) Juno spacecraft began its prime mission on 4 July 2016 when it started orbiting Jupiter on a highly elliptical 53-day polar trajectory (Bolton et al., 2017; Connerney et al., 2017). Near perijove, Juno skims above Jupiter's atmosphere at an altitude as low as 3,500 km above the cloud tops, while at the most distant point of its orbit, Juno reaches distances in excess of 100 RJ (1 RJ = 1 Jupiter Radius = 71,492 km). On every orbit, it rapidly passes over both polar regions at an altitude of a few Jovian radii, which is providing us with unprecedented viewing geometries of Jupiter's auroral emissions, while simultaneously measuring the particles and fields from whence the emissions originate. The Hubble Space Telescope (HST) campaign that is analyzed in the present study not only supports the Juno mission payload (particles, waves, magnetic field, and remote imaging/spectroscopy) and its science goals but it also provides crucial synergistic measurements and additional opportunities to augment the Juno mission science return relating to solar wind-magnetosphere-ionosphere coupling.

Jupiter's ultraviolet aurora comprises at least four components (e.g., Grodent, 2015, and references therein): Galilean satellite footprints, main emission (ME), emissions equatorward of the ME, and emissions poleward of the ME. It should be noted that the poleward and equatorward (antipoleward) directions that

we are using throughout this study for both hemispheres relate to the position of the magnetic pole, which we consider to be close to the geometric center of the ME contour. All these emissions relate to specific processes taking place in Jupiter's enormous magnetosphere. Since they are all observed simultaneously with HST, they are indirectly providing a global and dynamic picture of the Jovian magnetosphere. This HST campaign completes the local in situ information captured by Juno particles and field instruments and complements the Juno remote sensing instruments (see Bagenal et al., 2014; Bolton et al., 2017; Connerney et al., 2017; Mauk et al., 2017, and references therein, for the Magnetometer, Radio and Plasma Wave Sensor, Jovian Auroral Distributions Experiment, Jupiter Energetic particle Detector Instrument, Jupiter Infrared Auroral Mapper, JunoCam, and Microwave Radiometer instruments), particularly the Ultraviolet Spectrograph (UVS) (Gladstone et al., 2014, 2017).

During each Juno science orbit, UVS acquires science data for two short periods: near perijove for approximately 8 hr and near apojove for about one day but with low spatial resolution. For the remaining ~51 days of the orbit, that is more than 96% of the time, UVS is not observing the Jovian aurora. Therefore, for the majority of the time, there is no simultaneous ultraviolet observation of Jupiter's aurora with UVS, while other Juno in situ instruments are sampling the complex electromagnetic and particle environment to which the aurora is directly connected.

A similar HST campaign was executed in 2016 (GO-14105), at the time of orbital insertion of Juno, while its in situ instruments were measuring the conditions prevailing in the interplanetary medium (IM). This campaign allowed HST observations of Jupiter's auroras in response to upstream solar wind conditions, along with the first simultaneous in situ magnetic field and plasma measurements within the dawnside outer Jovian magnetosphere. The main results of this campaign were reported by Nichols, Badman, et al. (2017) and show that the IM likely triggers magnetospheric activity and subsequent auroral displays, but in a more complex way than previously thought. This is supported by the results presented by Kimura et al. (2015, 2017), Yoshikawa et al. (2017), and Bonfond et al. (2012) that the volcanic activity on Io is likely to significantly modify Jupiter's magnetosphere and generates recurrent strong transient auroral brightenings. However, it should be noted that we are still missing a clear connection between the enhancement of the activity of some volcanoes and the mass and energy balance of Jupiter's giant magnetosphere. These external and internal drivers appear to affect the auroral morphology differently. For the IM events, like the arrival of a compression region of a corotating interaction region or a coronal mass ejection, the ME and some features poleward of the ME are affected. For internal events related to Io and its plasma torus, it is mainly the emissions equatorward of the ME that show significant variations.

The main scope of the present study is to provide a simplified description of the global ultraviolet auroral morphology that can be used for comparison with other quantities, especially those obtained concurrently with various instruments onboard the Juno spacecraft, as well as with other space-based and Earth-based observatories. It is also meant to be used as a background, or starting point, for more detailed studies of specific auroral processes, such as the temporal behavior of some particular auroral features. We are taking advantage of the different responses of the aurora to external and internal conditions to link the morphology with the presumable state of the magnetosphere at the time of the HST observations.

In the following, we consider the HST data set that was collected concurrently with Juno during orbits 3 to 7. Section 2 describes this data set spanning an approximately eight-month period from 30 November 2016 to 18 July 2017. In section 3, in order to characterize the auroral activity, we define three subregions dividing the aurora according to its distance from the magnetic pole. The auroral emitted power is evaluated in these subregions as a function of time. In section 4, we define six morphological families that allow us to quantify the variations of the spatial distribution of the auroral emission. We relate these variations with the likely state of the Jovian magnetosphere, possibly influenced by the volcanic activity of Io and by the state of the upstream IM. For the latter, no instrument was measuring the solar wind conditions prevailing near Jupiter at the time of the present HST observations. Therefore, we can only estimate these characteristics from models propagating the solar wind measured near Earth to Jupiter, when the Sun, the Earth, and Jupiter are almost on the same line (e.g., Tao et al., 2005). The evolution of these auroral markers is then discussed in section 5 for each individual Juno orbit, from 3 to 7, with special focus on the two-week period bracketing the times of perijove referred to as PJ03 to PJ07.

2. Observations

All observations were obtained within the frame of HST program GO-14634. This large HST program takes advantage of the unique capabilities of the Space Telescope Imaging Spectrograph (STIS) UV camera, which provides a plate scale of 0.024 arsec^2 over an ~25 × 25 arsec^2 field of view. All observations shown here were made through the Far Ultraviolet-Multi-Anode Microchannel Array channel in time-tagged imaging mode with the F25SRF2 filter (~130–182.5 nm), which is used to prevent Ly-α contamination by geocoronal emission when HST is not in full occultation, and to reduce the amount of sunlight reflected by the Jovian planetary disk. Jupiter was positioned such that only the auroral region and a small portion of the Jovian disk illuminate the field of view of STIS. This ensures that the count rate always remains well below the bright-object limit. We obtained time-tagged exposures entirely filling the available HST orbital visibility period (~41 min), from which images integrated over smaller intervals (e.g., 10–100 s) are extracted to produce high-resolution movies of the Jovian auroral activity. For Jupiter, a time interval of 10 s is usually the shortest time globally providing sufficient contrast between the auroral signal and the planetary disk background. A 100 s interval increases the contrast for faint auroral structures but at the expense of temporal resolution. As a result, a 100 s interval is preferred to produce small size preview movies and still images. All images are calibrated and corrected for instrumental effects and background emissions, including planetary disk, by using the procedure described by Bonfond et al. (2011) and conversion factors provided by Gustin et al. (2012).

HST program GO-14634 is allocated 151 orbits, each of which usually consists of one visit. Some of these orbits are used to obtain spectrally resolved pseudo-images of Jupiter's aurora, while others are designed to observe atmospheric emissions of Jupiter's moons Io, Ganymede, and Europa. The spectral observations are not included in the present study and will be presented elsewhere. About three fourths of this HST program was dedicated to Juno orbits 3 to 7 and comprises the 118 visits reported here. The detailed characteristics of these visits are listed in Table 1 and in its more detailed version (Table S1 in the supporting information section). For the sake of clarity, each visit is assigned an index corresponding to the three middle characters of the official HST archive root name (for example, index "k01" for root name "od8**k01**r0q"). We note that these indices are not necessarily attributed in alphabetical order.

The present data set covers approximately eight months, spanning the 2016–2017 visibility period of Jupiter from HST. For the sake of time consistency, we subtracted 366 days to the "day of year 2017" (DOY) of data obtained in 2016, giving rise to negative DOY values in 2016. The first observation took place soon after HST's solar-avoidance period, during which the Sun is within 50° of Jupiter, on DOY −30, 11 days before perijove 3 (DOY −19). The last observation was obtained before HST's next solar avoidance, on DOY 199, one week after perijove 7 (DOY 192), when Jupiter was close to the opposite quadrature. Several observations were obtained close to Jupiter's opposition (DOY 97), near perijove 5 (DOY 86), when Jupiter was closest to Earth and STIS spatial resolution was highest (~80 km per pixel).

3. Auroral Power and Subregions

One of the most important characteristics of the aurora is its brightness. In the case of the UV aurora, the energy radiated by the auroral region is proportional to the energy that the atmosphere receives from charged particles, mainly electrons with energy exceeding 10 eV, impinging the top of Jupiter's atmosphere (e.g., Grodent et al., 2001). Therefore, there is a complex connection between the auroral brightness and magnetospheric processes that energize these incoming particles. The auroral brightness is highly dynamic, in both space and time. Brightness variations of several orders of magnitude are the norm for the Earth, but especially so for Jupiter's aurora, which fills a volume corresponding to several tens of times the volume of Earth, assuming that the vertical extent of Jupiter's auroral emission covers at least 1,000 km. Accordingly, it would be inappropriate to characterize the whole auroral region with one single brightness value representative of a particular region of the aurora that also depends on the viewing geometry, especially near the planetary limb (e.g., Gustin et al., 2016). This was dramatically illustrated during the previous HST program (Nichols, Badman, et al., 2017) in which images with strikingly different morphology exhibited similar total power values. For these reasons, we prefer to consider the auroral power emitted in each hemisphere, which informs us of the amount of energy

Table 1
List of Various Parameters Characterizing the 118 HST Visits Considered in This Study

Index	Rootname	HST time (dd/mm/yyyy)	HST DOY (2017)	Juno time (light corr.)	Hemisphere	CML start	Family
k01	od8k01r0q	30/11/2016 15:47:26	−30.3421	30/11/2016 14:57:23	N	146.100	X
k02	od8k02r4q	30/11/2016 17:22:48	−30.2758	30/11/2016 16:32:45	N	203.746	X
k05	od8k05vnq	1/12/2016 17:13:28	−29.2823	1/12/2016 16:23:32	S	348.537	X
k07	od8k07vrq	1/12/2016 18:48:52	−29.2161	1/12/2016 17:58:56	S	46.2033	i
k22	od8k22czq	2/12/2016 17:03:31	−28.2892	2/12/2016 16:13:41	N	132.958	N
k23	od8k23d1q	2/12/2016 18:38:54	−28.2230	2/12/2016 17:49:05	N	190.614	N
k26	od8k26q4q	4/12/2016 13:34:28	−26.4344	4/12/2016 12:44:51	S	307.470	Q
k11	od8k11fuq	5/12/2016 19:46:26	−25.1761	5/12/2016 18:56:58	S	322.756	X
k19	od8k19fwq	5/12/2016 21:21:49	−25.1098	5/12/2016 20:32:22	S	20.4128	I
k12	od8k12j9q	6/12/2016 14:51:43	−24.3808	6/12/2016 14:02:21	S	295.052	X
k20	od8k20jhq	6/12/2016 16:25:38	−24.3155	6/12/2016 15:36:16	S	351.822	i
k21	od8k21jtq	6/12/2016 18:01:00	−24.2493	6/12/2016 17:11:39	S	49.4689	i
k08	od8k08q5q	7/12/2016 16:16:40	−23.3218	7/12/2016 15:27:26	N	136.849	I
k03	od8k03t0q	8/12/2016 11:21:03	−22.5270	8/12/2016 10:31:54	N	108.604	N
k04	od8k04yuq	9/12/2016 12:46:53	−21.4674	9/12/2016 11:57:53	S	310.940	U
k06	od8k06ejq	10/12/2016 18:58:50	−20.2091	10/12/2016 18:10:00	S	326.231	U
k09	od8k09dmq	11/12/2016 17:14:00	−19.2819	11/12/2016 16:25:18	S	53.3173	U
PJ03			−19.2550				
k10	od8k10dxq	11/12/2016 19:18:02	−19.1958	11/12/2016 18:29:20	N	128.294	X
k17	od8k17e1q	11/12/2016 20:24:44	−19.1495	11/12/2016 19:36:02	N	168.613	i
k18	od8k18ljq	12/12/2016 15:29:12	−18.3547	12/12/2016 14:40:35	N	140.426	Q
k13	od8k13lus	12/12/2016 17:03:59	−18.2889	12/12/2016 16:15:22	N	197.721	Q
k15	od8k15qdq	13/12/2016 12:10:09	−17.4930	13/12/2016 11:21:37	N	170.564	Q
k14	od8k14vrq	4/12/12016 16:45:51	−16.3015	14/12/2016 15:57:27	N	127.685	I
k16	od8k16yrq	15/12/2016 08:39:04	−15.6395	15/12/2016 07:50:44	S	343.896	Q
k27	od8k27ghq	7/1/2017 01:57:08	7.08134	7/1/2017 01:11:38	S	322.353	U
k28	od8k28gpq	7/1/2017 03:32:30	7.14757	7/1/2017 02:47:00	S	20.0052	U
k25	od8k25jlq	22/1/2017 15:31:08	22.6466	22/1/2017 14:47:45	N	192.688	i
k29	od8k29fiq	23/1/2017 20:07:50	23.8388	23/1/2017 19:24:37	N	150.543	N
k30	od8k30i4q	24/1/2017 15:11:42	24.6331	24/1/2017 14:28:35	N	122.086	I
k31	od8k31iaq	24/1/2017 16:47:04	24.6994	24/1/2017 16:03:58	N	179.742	I
k33	od8k33xwq	26/1/2017 18:04:03	26.7528	26/1/2017 17:21:14	N	167.442	i
k34	od8k34apq	27/1/2017 13:08:24	27.5475	27/1/2017 12:25:42	N	139.284	N
k35	od8k35f8q	28/1/2017 09:48:08	28.4084	28/1/2017 09:05:33	N	168.793	N
k36	od8k36kkq	29/1/2017 14:24:36	29.6004	29/1/2017 13:42:11	N	126.527	I
k37	od8k37l0q	29/1/2017 15:59:58	29.6666	29/1/2017 15:17:33	N	184.183	I
k38	od8k38h7q	31/1/2017 07:43:57	31.3222	31/1/2017 07:01:47	N	185.487	I
k39	od8k39s3q	1/2/2017 12:20:26	32.5142	1/2/2017 11:38:26	N	143.240	N
PJ04			33.5687				
k44	od8k44ycq	2/2/2017 13:46:13	33.5738	2/02/2017 13:04:23	S	345.702	i
k45	od8k45yeq	2/2/2017 15:21:35	33.6400	2/02/2017 14:39:46	S	43.3592	i
k47	od8k47c1q	3/02/2017 08:50:35	34.3685	3/2/2017 08:08:50	S	317.568	i
k48	od8k48d2q	3/02/2017 13:36:40	34.5671	3/2/2017 12:54:56	N	130.530	N
k50	od8k50fqq	4/2/2017 10:16:26	35.4281	4/2/2017 09:34:48	N	160.076	N
k51	od8k51igq	5/2/2017 06:56:14	36.2891	5/2/2017 06:14:41	N	189.644	N
k52	od8k52diq	6/2/2017 11:32:56	37.4812	6/2/2017 10:51:31	N	147.544	i
k53	od8k53isq	7/2/2017 06:40:55	38.2784	7/2/2017 05:59:35	N	121.605	i
k54	od8k54iuq	7/2/2017 08:12:51	38.3423	7/2/2017 07:31:32	N	177.187	i
k55	od8k55tnq	1/03/2017 15:56:39	60.6643	1/3/2017 15:17:38	N	171.661	i
k56	od8k56o2q	5/03/2017 18:29:08	64.7702	5/3/2017 17:50:28	N	146.514	N
k32	od8k32anq	17/3/2017 08:39:23	76.3607	17/3/2017 08:01:34	N	158.011	X
k42	od8k42fiq	18/3/2017 14:52:23	77.6197	18/3/2017 14:14:38	N	174.219	X
k57	od8k57itq	19/3/2017 09:57:00	78.4146	19/3/2017 09:19:18	N	146.298	X
k58	od8k58eaq	20/3/2017 16:09:14	79.6731	20/3/2017 15:31:36	N	162.043	i
k59	od8k59huq	21/3/2017 11:13:44	80.4679	21/3/2017 10:36:09	N	134.051	i
k60	od8k60i1q	21/3/2017 12:49:06	80.5341	21/3/2017 12:11:31	N	191.713	i
k61	od8k61lyq	22/3/2017 07:53:33	81.3289	22/3/2017 07:16:01	N	163.691	i
k65	od8k65y9q	25/3/2017 05:49:37	84.2428	25/3/2017 05:12:14	N	180.793	N
k66	od8k66e3q	26/3/2017 15:12:12	85.6335	26/3/2017 14:34:54	S	311.630	i
k67	od8k67bfq	27/3/2017 03:55:05	86.1633	27/3/2017 03:17:49	S	52.8983	I

Table 1 *(continued)*

Index	Rootname	HST time (dd/mm/yyyy)	HST DOY (2017)	Juno time (light corr.)	Hemisphere	CML start	Family
k68	od8k68bxq	27/3/2017 05:30:26	86.2295	27/3/2017 04:53:10	N	110.550	I
k70	od8k70crq	27/3/2017 08:41:10	86.3619	27/3/2017 08:03:54	N	225.875	I
PJ05			86.3952				
k71	od8k71ctq	27/3/2017 10:16:32	86.4281	27/3/2017 09:39:17	S	283.537	I
k73	od8k73d1q	27/3/2017 13:27:15	86.5606	27/3/2017 12:50:00	S	38.8517	I
k72	od8k72g9q	28/3/2017 03:45:30	87.1566	28/3/2017 03:08:15	N	197.782	N
k74	od8k74hnq	28/3/2017 11:42:24	87.4878	28/3/2017 11:05:09	N	126.133	N
k75	od8k75hpq	28/3/2017 13:17:40	87.5539	28/3/2017 12:40:25	N	183.735	N
k76	od8k76lqq	29/3/2017 08:22:00	88.3486	29/3/2017 07:44:46	N	155.641	N
k77	od8k77opq	30/3/2017 03:26:22	89.1433	30/3/2017 02:49:08	N	127.567	N
k78	od8k78orq	30/3/2017 05:01:44	89.2095	30/3/2017 04:24:30	N	185.229	N
k79	od8k79u1q	31/3/2017 09:38:20	90.4016	31/3/2017 09:01:07	N	143.147	N
k81	od8k81roq	19/4/2017 19:27:01	109.810	19/4/2017 18:49:41	N	121.642	I
k82	od8k82ovq	23/4/2017 14:00:08	113.583	23/4/2017 13:22:41	N	166.553	I
k41	od8k41ixq	9/5/2017 06:42:14	129.279	9/5/2017 06:03:58	N	151.523	U
k63	od8k63neq	10/5/2017 06:32:53	130.273	10/5/2017 05:54:33	S	296.450	Q
k62	od8k62ogq	10/5/2017 11:19:00	130.472	10/5/2017 10:40:39	N	109.427	Q
k86	od8k86oiq	10/5/2017 12:53:48	130.537	10/5/2017 12:15:27	N	166.740	U
k64	od8k64rfq	11/5/2017 07:58:51	131.333	11/5/2017 07:20:26	N	138.998	U
k84	od8k84c6q	13/5/2017 09:15:18	133.386	13/5/2017 08:36:44	N	126.357	Q
k85	od8k85c8q	13/5/2017 10:50:40	133.452	13/5/2017 10:12:06	N	184.012	U
k87	od8k87d1q	15/5/2017 12:06:56	135.505	15/5/2017 11:28:13	N	171.244	Q
k87	od8k87d1q	15/5/2017 12:06:56	135.505	15/5/2017 11:28:13	N	171.244	Q
k88	od8k88hbq	16/5/2017 07:11:14	136.299	16/5/2017 06:32:27	N	143.034	I
k89	od8k89msq	17/5/2017 03:50:54	137.160	17/5/2017 03:12:03	N	172.476	U
k90	od8k90tpq	18/5/2017 08:27:19	138.352	18/5/2017 07:48:23	N	130.134	U
k91	od8k91txq	18/5/2017 10:02:40	138.419	18/5/2017 09:23:44	N	187.777	U
k94	od8k94x3q	19/5/2017 05:06:55	139.213	19/5/2017 04:27:56	N	159.529	N
PJ06			139.278				
k95	od8k95xgq	19/5/2017 06:42:17	139.279	19/5/2017 06:03:17	N	217.182	N
k97	od8k97xzq	19/5/2017 09:52:59	139.412	19/5/2017 09:13:59	S	332.469	I
k0a	od8k0ay5q	19/5/2017 11:28:19	139.478	19/5/2017 10:49:18	S	30.1020	I
k0b	od8k0bzxq	20/5/2017 01:46:31	140.074	20/5/2017 01:07:26	N	188.921	i
k0c	od8k0cgpq	21/5/2017 06:22:53	141.266	21/5/2017 05:43:41	N	146.535	N
k0h	od8k0hpgq	24/5/2017 04:18:33	144.180	24/5/2017 03:39:03	N	162.965	N
k0i	od8k0isyq	24/5/2017 23:22:50	144.974	24/5/2017 22:43:15	N	134.720	N
k0j	od8k0jt8q	25/5/2017 00:58:12	145.040	25/5/2017 00:18:37	N	192.372	U
k0k	od8k0kahq	26/5/2017 05:34:44	146.232	26/5/2017 04:55:01	N	150.064	U
k0l	od8k0le9q	27/5/2017 00:39:08	147.027	26/5/2017 23:59:20	N	121.883	N
k0m	od8k0meiq	27/5/2017 02:14:30	147.093	27/5/2017 01:34:42	N	179.534	N
k0n	od8k0nh8q	27/5/2017 21:18:55	147.888	27/5/2017 20:39:02	N	151.360	U
k69	od8k69idq	18/6/2017 09:55:28	169.414	18/6/2017 09:13:0	N	168.608	X
k0p	od8k0pg8q	4/7/2017 02:38:03	185.110	4/7/2017 01:53:41	N	150.776	N
k0q	od8k0qldq	5/7/2017 08:50:08	186.368	5/7/2017 08:05:37	N	166.062	Q
k0r	od8k0rniq	6/7/2017 02:19:12	187.097	6/7/2017 01:34:36	S	80.1525	U
k0s	od8k0sotq	6/7/2017 10:16:03	187.428	6/7/2017 09:31:24	S	8.37583	U
k0e	od8k0eqaq	7/7/2017 00:34:21	188.024	6/7/2017 23:49:38	N	167.159	Q
k0t	od8k0twqq	8/7/2017 05:13:19	189.218	8/7/2017 04:28:27	N	126.153	Q
k0f	od8k0fwuq	8/7/2017 06:46:16	189.282	8/7/2017 06:01:24	N	182.335	Q
k0u	od8k0uzgq	9/7/2017 01:50:36	190.077	9/7/2017 01:05:38	N	154.002	N
k0v	od8k0vfzq	10/7/2017 23:55:23	191.997	10/7/2017 23:10:12	S	25.1068	I
k0w	od8k0wgcq	11/7/2017 01:31:19	192.063	11/7/2017 00:46:08	S	83.0911	I
PJ07			192.107				
k0x	od8k0xhrq	11/7/2017 07:52:45	192.328	11/7/2017 07:07:31	S	313.638	i
k0y	od8k0yjqq	11/7/2017 23:46:17	192.990	11/7/2017 23:00:58	N	169.976	N
k0z	od8k0zs2q	13/7/2017 21:51:32	194.911	13/7/2017 21:05:57	S	41.3495	i
k1a	od8k1asqq	14/7/2017 01:02:15	195.043	14/7/2017 00:16:39	N	156.622	i
k1b	od8k1bubq	14/7/2017 05:48:18	195.242	14/7/2017 05:02:40	S	329.516	N
k1c	od8k1cuiq	14/7/2017 07:23:40	195.308	14/7/2017 06:38:02	S	27.1576	N
k1d	od8k1dwvq	15/7/2017 00:52:33	196.036	15/7/2017 00:06:49	S	301.121	N
k1e	od8k1ex2q	15/7/2017 02:27:54	196.103	15/7/2017 01:42:09	S	358.753	N

Table 1 *(continued)*

Index	Rootname	HST time (dd/mm/yyyy)	HST DOY (2017)	Juno time (light corr.)	Hemisphere	CML start	Family
k1f	od8k1fx8q	15/7/2017 04:03:16	196.169	15/7/2017 03:17:31	S	56.3938	N
k1g	od8k1gbkq	16/7/2017 02:18:14	197.096	16/7/2017 01:32:21	N	143.270	i
k1i	od8k1igpq	18/7/2017 03:34:19	199.149	18/7/2017 02:48:10	N	129.968	N

Note. The different columns of the table provide the index, the HST archive root name, the time at the start of the exposure (dd/mm/yyyy hh:mm:ss format), and the same time converted in decimal day of year (DOY) 2017; we subtracted 366 to observations made in 2016; the corresponding time at Juno corrected for light travel time (using the latest Juno trajectory kernels in SPICE), the observed hemisphere (N or S) Jupiter's central meridian System III (S3) longitude (CML) in degrees at the start of the exposure, and the morphological family. See also a more detailed version of this table in the supporting information (Table S1).

received from the magnetosphere at a given time. In parallel, we define six typical auroral morphological families (section 4) allowing us to characterize the overall distribution of brightness with one single descriptor. The emitted power is plotted in the different panels of Figure 1 and is discussed in section 3.5.

We also define three auroral subregions containing emission features of similar type and presumably sharing common magnetospheric origins. In the present analysis, there is no point in considering a larger number of smaller subregions, for instance, isolating the footprint of one particular satellite, since we aim to understand the global picture. (1) The ME is often referred to as the main oval, even though it never really forms a complete oval, especially in the northern hemisphere. (2) The *poleward region*, also known as the polar region, is bounded by the poleward boundary of the ME. (3) The *equatorward region* is defined by the equatorward boundary of the ME and the auroral footpath of Io, inclusive. They are named after their location in the ionosphere relative to the ME, and they are magnetically connected to different regions of the magnetosphere (e.g., Khurana et al., 2004), the usual names of which are inverted with regard to that of the subregions: the poleward subregion corresponds to the outer magnetosphere, the equatorward subregion corresponds to the inner magnetosphere, and the ME subregion corresponds to the middle magnetosphere.

These three subregions are illustrated in Figure 2 for the northern hemisphere; another set of subregions is defined for the southern hemisphere in the same way. They form three contiguous surfaces on Jupiter's ellipsoid, approximately centered on the geometrical center of the ME. The color code used in Figure 2 is the same as for Figure 1 (and Figures S1.1 and S1.3–S1.7), with the equatorward emission in yellow, the ME in red and the poleward region in green. The addition of these three regions encompasses the majority of the auroral emission in each hemisphere and is used to determine the total emitted power.

We set the width of the ME ribbon, the 2-D contour on Jupiter's surface roughly containing the ME, to 3,000 km (~2.5° on the surface of Jupiter) to make sure that the region encompasses the majority of the emission associated with the main aurora, while at the same time avoiding contamination by other types of emissions, that are ideally fully represented within the other subregions. This width is 5 to 10 times the typical width of the dawnside arc forming the ME. The efficiency of the subregion slicing largely depends on the quality of the definition of the contour best fitting the ME. Since the location of the main aurora may significantly change over a Jovian rotation, each visit is considered separately and we define a separate set of subregions for each observation. This approach is simpler than the method used by Nichols, Badman, et al. (2017), who further discriminate portions of these regions according to local time. The ME contour was also used to estimate the size of the aurora by assuming that it is reasonably represented by the area on the Jovian surface limited by the contour.

Since Jupiter's magnetic axis is tilted by only ~10° with respect to the spin axis, Earth-orbiting observatories can only capture one portion of Jupiter's aurora at the time. Therefore, we follow the methodology described by Bonfond et al. (2015) in which the closure of the contour is achieved with a Fourier series. This effect was also accounted for in Figure 1 and Table 1, where the emitted power is corrected for the viewing geometry by a time-dependent factor equal to the ratio between the total area of the subregion of interest and the area of its portion visible from Earth (Nichols, Clarke, Gérard, Grodent, & Hansen, 2009).

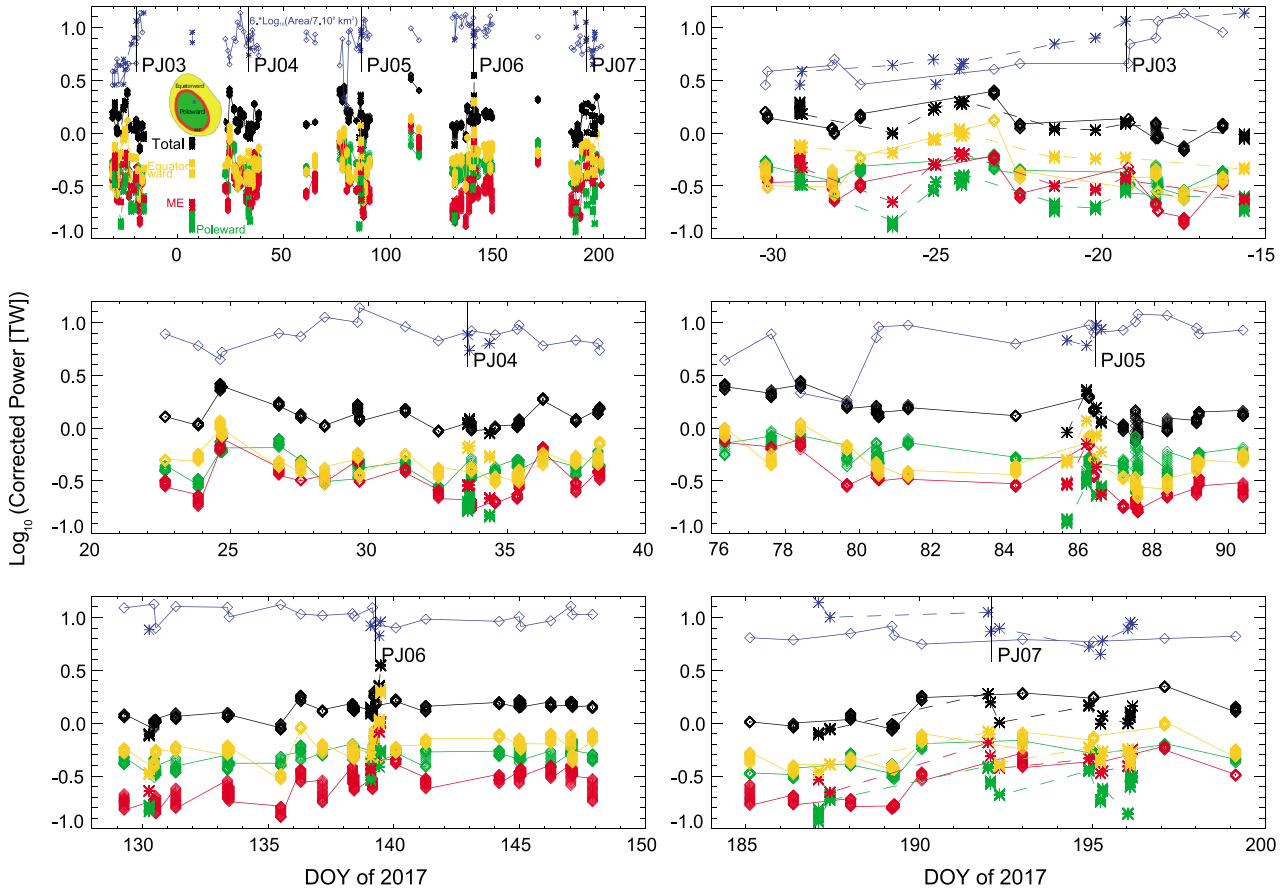

Figure 1. Auroral emitted power (TW) corrected for the viewing geometry as a function of time during the period covering Juno orbits 3 to 7, from 30 November 2016 to 18 July 2017. The time is given in decimal Day of Year 2017 (DOY). For observations obtained in 2016, we subtracted 366 days, resulting in negative DOY 2017. The times of perijoves 3 to 7, corrected for the Juno-HST light travel time, are marked with a vertical bar at the top of the plot. The upper left panel presents all the data in a single plot. A reduced version of Figure 2, depicting the color codes used for the poleward, equatorward, and ME subregions is overlaid in order to facilitate the reading of the different curves. Subsequent panels show the results for each individual orbit. The individual panels are also available in the supporting information (Figures S1.1 and S1.3–S1.7). The total power (black symbols and lines) is the sum of the power in the ME (red), poleward (green), and equatorward (yellow) subregions. Power values within each HST visits (~41 min) are averaged over 100 s, giving 24 data points per visit. The area of the planetary surface limited by the ME contour is represented with blue symbols and lines. We consider only one average value of the area per HST visit. The numerical value of the area was transformed in order to obtain numbers close to but larger than the total power, so that they can be conveniently displayed on the same logarithmic plot. The displayed value corresponds to $6 \times \mathrm{Log}_{10}(\mathrm{Area}/7 \times 10^8\ \mathrm{km}^2)$. The actual value of the area is given in Table S1 (supporting information) in units of $10^9\ \mathrm{km}^2$. All numbers referring to the northern hemisphere are marked with diamond symbols and connected with solid lines. Numbers referring to the southern hemisphere are marked with stars and connected with dashed lines. No definite long-term trend emerges from the general plot (upper left panel of Figure 1, see also Figure S1.1 in the supporting information). The corrected total power usually varies by a factor of 3 over time and remains between ~1 and 3 TW in each hemisphere. The dispersion of the total auroral power during one HST visit may be used as a proxy for the inaccuracy on the inferred emitted power.

3.1. Uncertainties on the Emitted Power

The intrinsic variability of the auroral emission power is well illustrated in Figure 1 by the vertical distribution of the data points over one HST visit (~41 min). During this time the subregion or total power may change by as much as one third. This level of variation is comparable to the estimated uncertainty on the emitted power, which is mainly influenced by three processes: the background subtraction, the conversion from STIS counts per second to emitted power, and the correction for the viewing geometry. The background subtraction procedure described by Bonfond et al. (2011) is based on the generation of a model planetary disk simulating the reflected sunlight. A conservative uncertainty of 25% on this simulation gives rise to ~6% inaccuracy on the auroral power. This inaccuracy is systematic and remains constant over an HST visit. Therefore, it is not affecting the relative variability of the emission. The conversion factor from STIS counts to emitted power depends on the emission spectrum passing through STIS + F25SRF2 filter optical assembly. It is affected by the amount of methane absorption, related to the energy of the impinging electrons through the H_2 UV color ratio

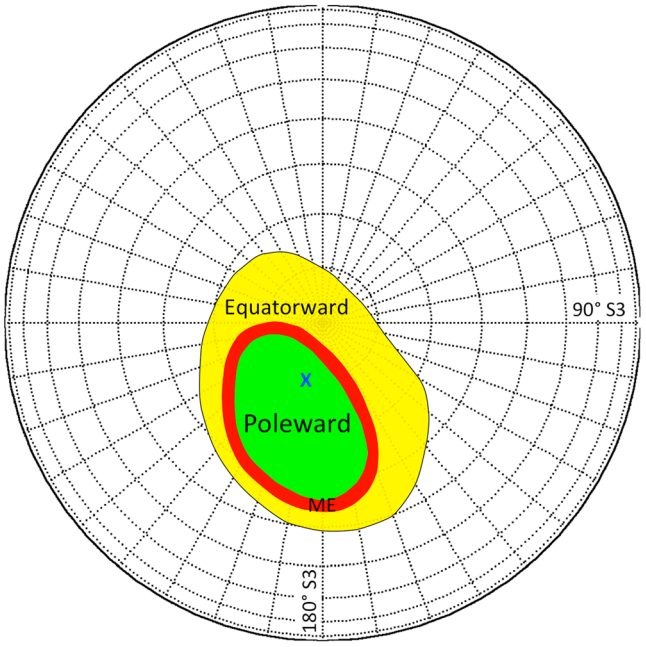

Figure 2. Definition of the three auroral subregions, for the northern aurora, containing emission features of similar type and presumably sharing common magnetospheric origins. We use the same color code as in Figure 1 to represent each subregion: (1) main emission (ME, red), often referred to as the main oval; (2) poleward region (green), also known as the polar region; it is bounded by the poleward boundary of the main emission; and (3) equatorward region (yellow), defined by the equatorward boundary of the main emission, and includes the auroral footprint of Io. They form three contiguous surfaces on Jupiter's ellipsoid, approximately centered on the geometrical center of the main emission. The addition of these three regions encompasses the majority of the auroral emission in each hemisphere and is used to determine the total emitted power. The poleward subregion corresponds to the outer magnetosphere, the equatorward subregion corresponds to the inner magnetosphere, and the ME subregion corresponds to the middle magnetosphere. Another set of three subregions is defined for the southern hemisphere in the same way. We set the width of the main emission ribbon, the 2-D contour on Jupiter's surface roughly containing the main emission, to 3,000 km (~2.5° on the surface of Jupiter). The blue cross marks the location of the magnetic dipole.

described by Gustin et al. (2012). In the present study, we have assumed a constant color ratio of 2.5, while, following Gérard et al. (2014, 2016) and Bonfond et al. (2017), this color ratio is found to vary significantly with space and time. We note that a color ratio of 1.5, corresponding to a weak level of absorption would decrease the conversion factor by 7% and a color ratio of 5, corresponding to a relatively strong absorption by methane, would increase the factor by about the same amount. Finally, as a result of the viewing geometry from Earth orbit, we usually capture around two thirds of the auroral region. This is corrected by a geometry factor assuming that the average emission brightness in the hidden part of the auroral subregions, defined above, equals the average brightness measured in the visible portion of the corresponding subregions. The uncertainty brought by this correction may be estimated by assuming that the power emitted by the one third of the aurora that is not visible to HST is affected by a variability of 33%, like the rest of the emission, leading to an imprecision of ~10%. Like the background disk subtraction, this uncertainty is rather systematic and does not alter the intrinsic variability of the auroral emission over one HST visit. The total (quadratic) uncertainty is thus on the order of 14%, smaller than the intrinsic auroral variability. The measured variability of the emission during one HST visit is thus real and the dispersion of the data points over one visit in Figure 1 is, in most cases, a relatively good indicator of the inaccuracy on the inferred auroral emission power.

3.2. The ME Subregion

The ME subregion contains the emission likely associated with the process of corotation breakdown in the middle magnetosphere (e.g., Cowley & Bunce, 2001; Hill, 2001). It is tightly linked to the magnetic field topology, and the subregion remains fixed in the System 3 (S3) frame of reference, rotating with it. It should be noted that while the bulk of the auroral emission, and therefore the subregions, are fixed in S3, the emission inside these subregions may not be strictly corotating with the planet and display local time morphological variations giving rise to redistribution of the emission along the subregions (Grodent, Clarke, Kim, et al., 2003; Grodent, Clarke, Waite, et al., 2003). Bonfond et al. (2015) showed that, statistically, the ME is brighter on the duskside than on the dawnside. As already suggested above, this emission does not form a continuous ribbon of emission but rather an assemblage of extended features influenced by the position of the Sun. On the dawnside, these features usually form a well-defined ME often taking the form of a narrow arc. In the prenoon sector, the brightness rapidly drops, giving rise to a discontinuity (Chané et al., 2013; Radioti et al., 2008), often followed by a brighter spot (Nichols, Yeoman, et al., 2017; Palmaerts et al., 2014). In the afternoon sector of the northern hemisphere, the ME takes a more dynamic form, presumably influenced by the presence of a potential high-latitude magnetic anomaly (Grodent et al., 2008; K. M. Moore et al., 2017) acting like a magnifying glass and revealing the intricate morphology of the ME. This anomaly is fixed in S3 but for observations from Earth orbit, the viewing geometry is such that it appears in the afternoon sector. In the southern hemisphere, it is likely that no such anomaly exists and the ME consists of more regular arc-like features. We emphasize that the magnetic field of Jupiter is far from symmetric and N-S auroral asymmetries have been reported by Gérard et al. (2013). It is in this anomaly sector that the ME is more likely to be contaminated by or to contaminate the features of the other subregions. The ME emission is usually stable in time, at least for the duration of an HST visit, but at times, strong brightenings of the dawnside ME, often referred to as dawn storms (Clarke et al., 1998; Gustin et al., 2006), occur with shorter timescales. The ME power is plotted in Figure 1 and discussed in section 3.5, along with the other subregions. According to the different studies of Nichols et al. (2007); Nichols, Clarke, Gérard, Grodent, and Hansen (2009); and

Nichols, Badman, et al. (2017), it is expected that the ME subregion power is measurably sensitive to the conditions in the IM. Specifically, the power of the dawn sector of the ME was shown to increase significantly following compression region onset. According to the three-dimensional one-fluid magneto-hydrodynamic (MHD) global simulations of Chané et al. (2017), such an enhancement of the dawn emission during the solar wind compression could be a result of larger magnetic stresses exerted on the magnetosphere caused by increased solar wind ram pressure.

3.3. The Poleward Subregion

The poleward subregion contains the most variable components of the Jovian aurora (Grodent, Clarke, Waite, et al., 2003). Their poleward location suggests that they are associated with the outer magnetosphere, extending to the magnetopause, and possibly with open magnetic field lines (Vogt et al., 2015), although it is still unclear how the solar wind exchanges momentum and energy with Jupiter's magnetosphere (Delamere et al., 2014, 2015). Grodent, Clarke, Waite, et al. (2003) divided this subregion into three smaller regions (dark, swirl, and active) characterized by different auroral dynamical behaviors and the boundaries of which are affected by the subsolar longitude. In that regard, Nichols, Badman, et al. (2017) recently refined the selection with the dusk active region (DAR) and noon active region, respectively. Bonfond et al. (2016) performed a detailed analysis of the active region and reported quasiperiodic brightness variations on a 2 min timescale as well as propagation of fast wave-like auroral features, the origin of which is still uncertain. The poleward subregion also contains a recurrent polar auroral filament (Nichols, Clarke, Gérard, & Grodent, 2009), which is superficially similar to terrestrial transpolar auroral arc (or "theta" aurora). At Earth, their generation is usually associated with magnetic reconnection process (e.g., Fear et al., 2014). Nichols, Badman, et al. (2017) suggested that the DAR is affected by the IM activity, with significantly enhanced and pulsing emission features, arcs and patches, which affects the power in the poleward region accordingly. Since in the present study we are interested in the global auroral morphology, we do not address the details of the very complex ingredients that are filling the poleward subregion. Instead, we focus on the longer-timescale power variations.

3.4. The Equatorward Subregion

The equatorward subregion contains the rest of the auroral emission bounded by and including the auroral footpath of Io. This includes the satellite footprints and their different components (Bonfond, Grodent, et al., 2017), the diffuse secondary emission (SE) (Gray et al., 2017; Radioti et al., 2009), and the auroral signatures of magnetospheric plasma injection (Bonfond et al., 2012; Dumont et al., 2014; Gray et al., 2016; Kimura et al., 2015). It is therefore likely that the equatorward subregion corresponds to the dynamics from the inner to middle magnetosphere. Very often, these three types of equatorward auroral features mix together, which raise difficulties in discriminating them. This is particularly unfortunate for the studies of the weak footprints of Ganymede and Europa, whose signatures are often drowned out by the SE and/or the injection signatures. In addition, Bonfond et al. (2012) showed that under some conditions, the ME may move equatorward of the footprint of Ganymede, the latter thus contributing to the ME subregion. However, the total power emitted by the satellite footprints is small in comparison with the other components, and such change would remain unnoticed in Figure 1. This is also true for the short quasiperiodic variations of the satellite footprint. In general, the substantial enhancements of the equatorward subregion power may be attributed to the injections. Bonfond et al. (2012) and Yoshikawa et al. (2017) suggested that there is an indirect link between the volcanic activity of Io and the occurrence rate of such large injection signatures, where an enhanced volcanic activity would be associated with an increased plasma loading of the middle magnetosphere which in turn favors flux tube interchange and increases the rate of injection of sparse hot plasma in the inner-middle magnetosphere.

3.5. Power Variations During the Campaign

Several pieces of information may be drawn from the busy light curves displayed in the upper left panel of Figure 1. First, no clear long-term trend emerges from this plot. The corrected total power (solid black line for the north, dashed black line for the south) usually varies by a factor of 3 and remains between ~1 and 3 TW in each hemisphere, with the exception of two rare events on DOY 109.806 (visit k81) near apojove 5, observed in the northern hemisphere, and DOY 139.478 (visit k06) near perijove 6, in the southern hemisphere. During these events, the total power reached extreme values in excess of 3.5 TW (see also power

values in Table S1 in the supporting information). In both cases, the large emission power resulted from an episode of very strong injection signatures within the equatorward subregion (yellow line, solid for the north, dashed for the south in Figure 1) combined with enhanced emissions in the ME subregion (red line, solid for the north, dashed for the south). In both cases, the poleward subregion was not particularly bright (solid and dashed green lines), suggesting that the aurora in the poleward subregion is disconnected from the other components. In general, the contribution from the three subregions (i.e., ME, poleward, and equatorward) to the total power is on the same order of magnitude, and as a rule of thumb, it may be stated that during unperturbed periods, each subregion approximately contributes one third of the total power. This rule breaks down during extreme events such as during visit k06, described above, where the distribution was 15% (poleward), 30% (ME), and 55% (equatorward). Within one visit (~41 min.) the power changes very rapidly, by amounts of a few hundreds of GW over ~100 s up to 500 GW during events characterized by enhanced contribution from the poleward subregion, which contains the most variable auroral features (Bonfond et al., 2016).

Interestingly, variations of the area of the surface subtended by the ME contour (upper blue lines in Figure 1, dotted in the north, dashed in the south) are anticorrelated with variations of the total power, suggesting that stronger power is associated with smaller auroral region (Badman et al., 2016; Nichols, Clarke, Gérard, Grodent, & Hansen, 2009). The linear correlation coefficient is −0.36 in the northern hemisphere and −0.33 in the southern hemisphere, corresponding to moderate anticorrelations.

Comparison of the total power in the northern and southern hemispheres, when we captured both close in time, that is for the eight pairs of visits taken less than 5 hr apart, shows no clear systematic trend, which is partly expected from the very large variability of the aurora. However, we note that the power in the poleward subregion is systematically smaller in the south than in the north, with south-north power ratios ranging from 0.28 to 0.83, even for the cases where the ratio is reversed for the other subregions (south more powerful than north). At present, this discrepancy remains unexplained.

In the following, we introduce the typical auroral morphologies that have been recorded during this first part of the HST-Juno campaign.

4. Typical Morphologies and Auroral Families

The bulk morphology of Jupiter's UV aurora is known to change rapidly, usually within one Jovian rotation and sometimes during a period of time as short as a few hours. In addition, the features of smaller scale structures such as the satellite footprints or isolated auroral patches within the polar region can also display substantial variations on the minute or even shorter timescales.

As a result, it would be deceptive to select an image that is fully representative of a whole Juno orbit (53 days), a particular day, or even of a perijove sequence (~6 hr). Instead, we selected one visit for each Juno orbit, in the northern hemisphere, for a central meridian longitude (CML) close to 143° S3, which is offering a relatively complete view of the various auroral components. The choice of CML was dictated by two criteria: first the availability of an HST visit at that particular CML ±3°, in order to compare auroral morphologies captured with almost exactly the same viewing geometry, and second the variety of morphologies, in order to display an indicative sample of typical morphologies.

Figure 3 shows six sample frames displayed with the same logarithmic color table so that they may be directly compared with each other. The six selected visits all show the same basic auroral ingredients, but with different proportions. In some cases, these differences may be dramatic and sudden, suggesting that the magnetosphere and the coupled ionosphere are regularly undergoing large-scale changes. The complexity of the auroral morphology is such that no two observations are alike and they seem to display an ever-changing auroral landscape. Still, in this apparent chaos, some recurrent patterns emerge and these selected morphologies allow us to define six auroral "families." However, we note that the discrimination between these families carries some elements of subjectivity, and in some cases, the observed morphology may fit several families or eventually none. As discussed below, each auroral family (Quiet [Q], Unsettled [U], Narrow [N], moderate injections [i], strong Injections [I], and eXternal perturbation [X]) may tentatively be related to a certain state of the magnetosphere, which itself is influenced by internal and external drivers, such as the amount of plasma transport from the Io torus or the local dynamic pressure of the IM, respectively. These

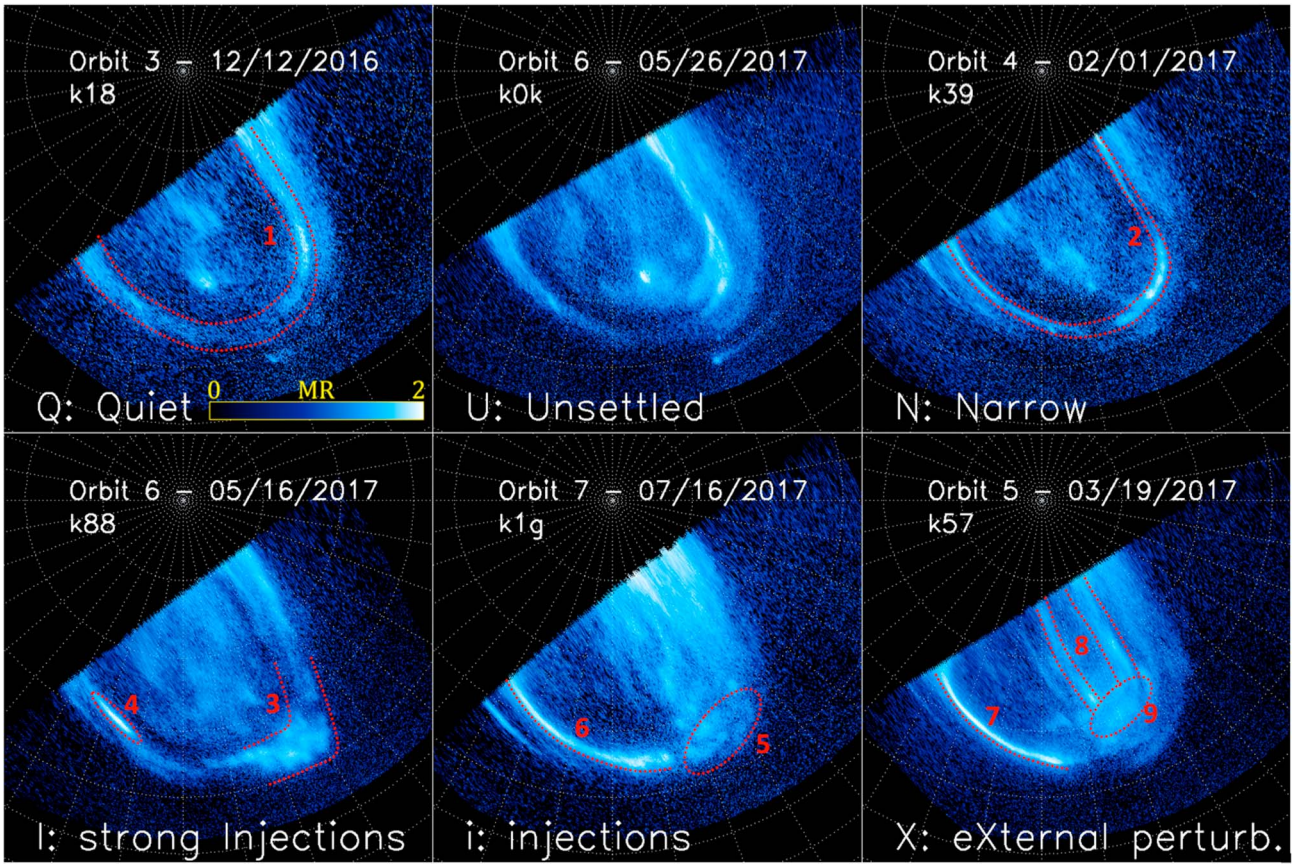

Figure 3. Illustration of the six morphological auroral families defined for Jupiter's northern aurora. The aurora, accumulated for 100 s, is projected on a polar map with 10° spaced S3 meridians (180° to the bottom, 90° to the right) and parallels, assuming an emission altitude of 400 km. The same saturated log-scale blue hues color table is used in each individual panel and adjusted to increase the contrast of the different auroral components. A color bar saturating at 2 MRayleighs is overlaid to the upper left panel. The six selected visits (k18, k0k, k39, k88, k1g, and k57) all display the same basic auroral ingredients but with different proportions. Each auroral family (Q, U, N, J, i, and X) displayed in the corresponding panel is potentially representative of a certain state of the magnetosphere, which itself is influenced by internal and external drivers. These family codes are used in Table 1 and repeated in Table 2; they allow one to easily trace the evolution of the auroral morphology during the period covered by this HST campaign. Similar families were defined for the southern hemisphere, for which the viewing geometry is usually less favorable than for the northern hemisphere. We selected at least one visit for each Juno orbit, in the northern hemisphere, for a CML close to 143° S3, which is offering a relatively complete view of the various auroral components. The availability of observations at this CML (±3°) makes it possible to compare auroral morphologies captured with almost exactly the same viewing geometry. Auroral features characterizing different morphologies are highlighted with red dashed lines, and ellipses and red numbers from "1" to "9." For example, the corner-shaped feature marked "3" in the lower left panel is typical of the strong injections (I) family.

family name codes are used in Table 1 (and Table S1). With the light curves displayed in Figure 1, they allow one to easily trace the evolution of the auroral morphology during the period covered by this HST campaign. Again, since most of the data were collected during approximately one-week periods centered on the times of Juno perijove, and considering the important variability of the aurora, the morphological tracing is obviously limited to these periods. Similar families were defined for the southern hemisphere, for which the viewing geometry is usually less favorable than for the northern hemisphere. Accordingly, categorization in southern families is less reliable, although images taken close in time in both hemispheres turn out to belong to the same family. The following paragraphs describe the main characteristics of each family, based on a sample of data in the northern hemisphere. These characteristics are also conveniently summarized in Table 2.

4.1. The Q ("Quiet") Family

The Q family example displayed in upper left panel of Figure 3 appeared in visit k18 (Table 1), on 12 December 2016 (DOY −018), about one day after perijove 3. The main characteristic of this morphology is the very low emission power (total less than 1 TW) of most auroral components, especially those filling the

Table 2
Main Characteristics of the Six Morphological Families Used in This Study

Name	Code	Index	Frequency	Auroral characteristics
"Quiet"	Q	1	11%	Overall low auroral power, expanded broad ME
"Unsettled"	U	2	29.5%	Intermediate between Q and N
"Narrow"	N	3	8.5%	Very narrow ME, average power
"injections"	i	4	18%	Moderate injections signatures, continuous ME
"strong Injections"	I	5	18.5%	Strong injections signatures, corner shape, disrupted dawnside ME
"eXternal perturbation"	X	6	14.5%	Strong dawnside ME, contracted ME, poleward strong parallel arcs

ME and equatorward subregions. Comparison with the upper middle panel reveals that in this case, even the auroral footprint of Io is dimmer. The ME is barely visible (marked "1" in Figure 3) so that the ME is not well defined. In particular, there is no apparent arc feature on the dawnside of the ME, but a rather diffuse and wide ribbon of emission. As a result, the faint ME discontinuity can hardly be discriminated, although we observe the expected continuous dimming of the emission from dawn to noon. The ME contour is particularly extended, as indicated by the peaking value of the area of the surface it subtends (blue top curves in Figure 1). We note that although the power in the poleward subregion is also very low, the associated time tagged movie shows that there is still a lot of polar activity with successive spot flashings and wave-like propagating features. As expected, the main contribution to the total power is coming from the poleward and equatorward subregions. However, the power in the equatorward subregion remains small, compared to other visits, suggesting that there is no ongoing large-scale injection. Overall, the low power and the absence of a sharp dawn ME suggest that a large portion of the magnetosphere was likely in an undisturbed state (see discussion in section 5.4 and correlation of such morphology with observed low upstream solar wind activity by Nichols, Badman, et al., 2017), presumably with very little plasma to bring back to corotation. This family occurs about 11% (13 out of 118) of the HST visits and spreads over all Juno orbits.

4.2. The U ("Unsettled") Family

The U family is illustrated with case k0k in upper middle panel of Figure 3, on 26 May 2017 (DOY 146), one week after perijove PJ06. It is intermediate between the Q and N families as the dawn ME sector emission is relatively wide and faint. On the contrary, in the afternoon sector, the ME is usually brighter and narrower. The equatorward emission is also faint, sometimes forming a distinct SE, parallel and equatorward of the ME. According to Radioti et al. (2009), this SE is not necessarily associated with signatures of plasma injections, but could be caused by a dipolarization of the magnetic field beyond the orbit of Europa, creating the conditions for producing whistler mode waves that are able to scatter the plasma sheet electrons in the loss cone and produce aurora. The poleward subregion aurora is similar to what is observed for the N family, suggesting that apart from the X family, this subregion behaves independently from the rest of the emission. The U family has a frequency of 14.5%, comparable to Q and I. Like the Q family the ME contour of the U family is extending more equatorward and subtends a rather large surface, which, according to Nichols, Badman, et al. (2017), may be associated with a rarefaction region in the IM.

4.3. The N ("Narrow") Family

The N family example displayed in the upper right panel of Figure 3 corresponds to visit k39, obtained on 1 February 2017 (DOY 032), one day before perijove PJ04. The total power is also relatively low, but in this case the morphology is characterized by a very narrow dawnside ME arc (marked "2" in Figure 3) with a width (Gaussian fit full width at half maximum) on the order of 200–300 km, very close to STIS' Point Spread Function. The rest of the ME also consists of relatively narrow arcs, giving rise to a quasi-continuous ME. Brightness values along the ME are average, leading to a sharp discontinuity in the 10:00–12:00 LT sector. The activity in the poleward subregion is somewhat similar to that observed for the Q family, but the power increases proportionally with the ME subregion power. The power in the equatorward subregion is relatively low as it mainly contains faint auroral signatures of injections, possibly remnants of previous stronger emissions. Most N family members show an expanded ME. About 29.5% of the visits match this family, making it the most frequent one. Like Q family, the N family may also correspond to a quiet magnetosphere but with a slow mass loading increase that may lead to the need for moderate plasma acceleration and a corresponding

slight enhancement of the field-aligned currents related to the ME aurora through the process of corotation enforcement.

4.4. The I ("Strong Injections") Family

The lower left panel of Figure 3 shows an example of the "strong Injections" family, or I family, with k88, obtained on 16 May 2017 (DOY 136), three days before perijove PJ06. The unmistakable characteristic of the members of this family is the very strong enhancement of the emission near longitude 150° S3, equatorward of the ME (marked "3" in Figure 3) and associated with the dynamics in the inner magnetosphere, which is likely associated with magnetospheric plasma injections and is worth a more detailed description. These emissions are the main contributor to the equatorward subregion, the power of which can easily surpass the power in other subregions. Hence, the most noticeable feature of this enhancement is its nonuniform meridional distribution, which contrasts with the statistical analysis of Dumont et al. (2014), who show that this emission is, on average, evenly distributed in longitude and does not show preferential local time. For the I family, the emission often forms a recurrent pattern (mostly in the northern hemisphere) with an accumulation in the 140–170° S3 region, resulting in a low-latitude corner-shaped feature ("3" in Figure 3) contrasting with the rest of the emission. This morphology may therefore be only associated with the few episodes of very strong plasma injection. We note that in the southern hemisphere, this region is located at lower S3 longitudes ranging from 40 to 100°. This emission is almost fixed in S3, with a very slight drift in longitude and latitude. Within this structure, there are sharp brightness discontinuities and the brightness itself is either increasing or decreasing with time, with different time scales for different substructures. A second characteristic of the I family is the broken appearance of the ME and the presence of localized, short-lived (less than a Jovian rotation) dawn brightenings (marked "4" in Figure 3), sometimes very strong. The latter have often been referred to as "dawn storms," although there is still no clear definition of these recurrent features. In the present family, these slightly subcorotating brightenings are found on the ME. Yao et al. (2017) suggested that similar auroral features observed at Saturn are consistent with a process of internally driven corotating reconnection. On the afternoon side, contrary to the X family, the ME is not particularly well defined. In some cases, it is even totally absent.

This family is reminiscent of the sudden auroral brightenings discussed by Kimura et al. (2015) and of the morphology discussed by Bonfond et al. (2012), Badman et al. (2014), Gray et al. (2016), and Nichols, Clarke, Gérard, Grodent, and Hansen (2009), suggesting that it is rather common, as confirmed by the measured frequency of 18%. This is compatible with Kimura et al. (2015), who derived a frequency of one such event every 4.7 days. In the present sample, the poleward subregion of the I family is not particularly bright or dim, suggesting that the poleward and equatorward subregions are disconnected. Kimura et al. (2015) showed that these strong equatorward subregion emissions may occur during periods of quiet solar wind activity. Bonfond et al. (2012) tentatively associated periods of repeated strong equatorward emission events every few days over periods of several weeks. Using Hisaki observations, Yoshikawa et al. (2017) showed that the brightness of short lived events (~10 hr) associated with equatorward emissions increased approximately two weeks after the beginning of an intense volcanic event on Io. Such enhancements probably result from the progressive ionization of logenic volcanic material, which increased the amount of outward moving heavy flux tubes that must be replaced by hot plasma, therefore increasing the occurrence rate of large features associated with bright injection signatures. During its first perijove sequence, Juno UV observations showed the progressive development of intense equatorward emissions possibly associated with injections, followed by the emergence of a protrusion inside the ME possibly related with internal reconnection in the tail (Bonfond, Gladstone, et al., 2017). Yoshikawa et al. (2017) and Bonfond, Gladstone, et al. (2017) thus suggest that injections of hot plasma precede internally driven reconnection events.

4.5. The i ("Moderate Injections") Family

The i family is represented in lower middle panel of Figure 3 with k1g, captured on 16 July 2017 (DOY 197), five days after perijove PJ07. The morphology resembles that of family I. The major difference stems from the lower brightness of the equatorward subregion features ("5" in Figure 3) and the absence of equatorward ME brightenings, resulting in narrow dawn ME arcs ("6" in Figure 3), often bright, somewhat similar to what was observed in the X family. It is likely that the i family represents a later or earlier stage of the I family, where the

signatures of plasma injections continuously increased then decreased, down to the point where the power in the equatorward subregion may be smaller than in the other subregions. Like in the I family, the afternoon side ME is not well defined and sometimes absent. The power in the poleward subregion is equivalent to that in the I family, with occasional very strong brightenings in the afternoon sector of the polar region. About 18.5% of the present sample fit in the i family. Put together with the I family, these injection cases represent more than one third of the data set.

4.6. The X ("eXternal Perturbation") Family

A member of the X family is shown in lower right panel of Figure 3. Visit k57 was taken on 19 March 2017 (DOY 78), more than a week before perijove PJ05. This family is distinguishable mostly for its very strong dawnside ME (marked "7" in Figure 3), which forms a very bright and narrow arc that has a sharp boundary with the discontinuity region, near 10:00 LT. In this regard, in case of a compressed magnetosphere, the MHD model of Chané et al. (2017) generates larger magnetic stresses and associated modified field-aligned electric currents, which are consistent with a more pronounced discontinuity. In more than half of the cases, the afternoon side of the ME is also bright and narrow, leading to a strong ME. As a result, the power in the ME subregion is usually the largest contributor to the total emitted power. However, in more than 70% of the cases, the poleward subregion is also filled with bright polar emissions, mainly on the duskside, corresponding to features marked "8" and "9" in Figure 3, suggesting a possible connection between the brightenings in these two subregions. Nichols, Badman, et al. (2017) suggested that such brightening of the ME and duskside polar region is a response to an external perturbation taking the form of a compression region in the IM, but the physical mechanism remains poorly understood. The typical auroral morphology observed during these periods also comprises "bright, strongly pulsing patches or arcs parallel" to the ME in the dusk sector of the poleward subregion (the DAR region defined by Nichols, Badman, et al., 2017). We note that the majority of the X family members also exhibit this typical auroral feature. Therefore, we suggest that the X family is representative of Jovian auroral response to enhanced IM activity. On the contrary, the equatorward subregion power is low compared to the other two regions, indicating that it is probably independent from the IM activity, as expected from an internal origin, indicating that the stress exerted by the IM activity acts less in the inner magnetosphere. The frequency of the X family is 8.5%, close to that of the Q family, suggesting that they are both rather exceptional conditions.

A few visits defy any categorization. For three of them (k46, k49, and k93) the poor viewing geometry prevents us from seeing enough auroral features to select a family. In the case of k24, the diffuse morphology approximately fits the Q family, but the total emitted power is large (a factor of ~2) compared to the rest of the family. Those visits were not included in this analysis.

5. Discussion on the Evolution of the Auroral Morphology and Power

A graphical representation of the evolution of the auroral morphology over Juno orbits 3 to 7 is given in Figure 4 (see also individual parameters in Table 1 and characteristics in Table 2 and enlarged versions of Figure 4 panels in the supporting information). Each family was assigned a qualitative index: Q = 1, U = 2, N = 3, i = 4, I = 5, and X = 6. This index somewhat reflects the typical power level measured in the families and is also such that the indexes of related families, like i and I, differ by 1 unit and very different morphologies, like X and Q, have very different values. This qualitative index allows us to provide a graphical representation of the importance of the morphological changes of the aurora with time. Morphologies observed in the north are marked with a diamond, and those observed in the south are marked with a star. Interestingly, some trends emerge from this plot as the typical morphologies observed around the times of perijove 3 to 7 change noticeably. These differences presumably stem from global variations of the internal (Iogenic) and external (IM) conditions, so that the present HST data set indeed provides one with a global auroral context during this eight-month period, from which the magnetospheric backdrop may be inferred.

5.1. Juno Orbit 3

During the two-week period including perijove PJ03 (DOY = −19.26), the auroral morphology rapidly and repeatedly changed from the extreme X to Q families, through all other families (Figures 4 and S4.3). Very close to perijove, the X auroral morphology was typical of a magnetosphere perturbed by an IM

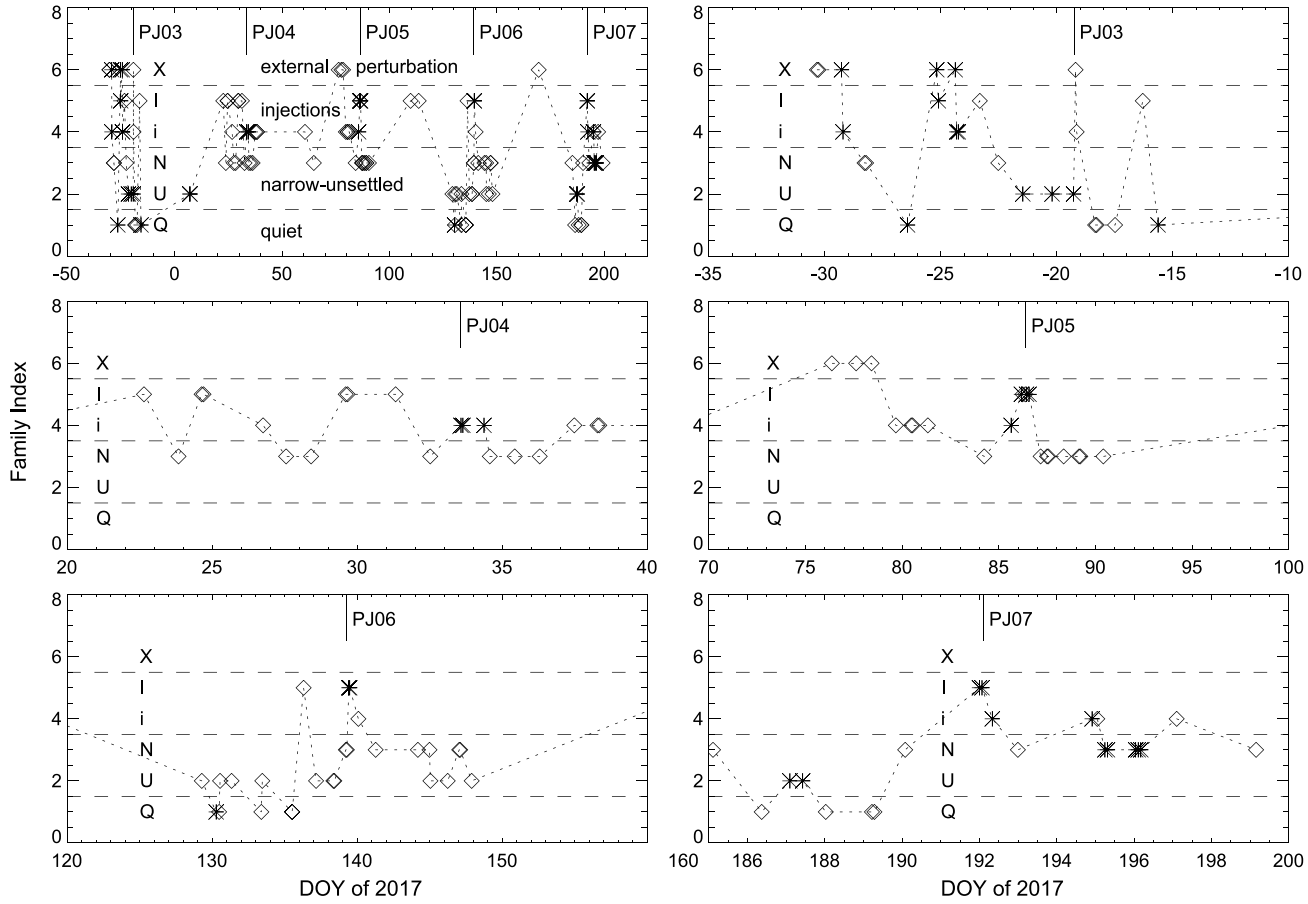

Figure 4. Graphical representation of the evolution of the auroral morphology over Juno orbits 3 to 7 (see also detailed parameters in Table 1). Like Figure 1, the upper left panel presents all the data in a single plot, while the subsequent panels show the results for each individual orbit. The individual panels are also available in the supporting information (Figures S4.1 and S4.3–S4.7). Each family is assigned a qualitative index: Q = 1, U = 2, N = 3, i = 4, I = 5, and X = 6. This index reflects the typical power level measured in the families and is also such that the indexes of related families, like I and i, differ by 1 unit. Morphologies observed in the north are marked with a diamond, and those observed in the south are marked with a star. The time is given in decimal DOY 2017. For observations obtained in 2016, we subtracted 366 days, resulting in negative DOY 2017. The times of perijoves 3 to 7, corrected for the Juno-HST light travel time, are marked with a vertical bar at the top of the plot. The horizontal dashed lines are guiding lines. The upper one separates the X family, influenced by the external perturbations, from the strong and moderate injection I and i families, influenced by plasma injections. The lowest line separates the Narrow and Unsettled (N and U) families, corresponding to the most frequent auroral morphologies, from the Quiet (Q) family, characterized by very low emitted power.

compression, while the day after the aurora had dropped to the opposite Q morphology, presumably corresponding to an unperturbed magnetosphere and stayed in that state for a day or two, followed by a new episode of strong injections. During the week that preceded PJ03, the magnetosphere might have encountered more than one IM compression regions and saw several episodes of strong injections, both of which contributed to a rapidly changing morphology. These morphological changes have an impact on the emitted power, as shown in Figure 1 (and Figure S1.3). During the same period, the total emitted power varied by a factor of ~3 from 0.7 to 2.4 TW. The largest power was emitted during the week preceding PJ03, when the very strong emissions in the equatorward subregion combined with the enhancement of the ME subregion. The smallest power was observed for the Q family members. Near the time of perijove, the total power peaked to 1.36 TW and rapidly dropped to its minimum at 0.7 TW, which is also the smallest value measured during the period covered by this study. It is interesting to note that the power emitted in the poleward subregion followed the same trend as in the ME subregion. This is surprising since these two subregions are presumably mapping to very different regions of the magnetosphere and, so far, were expected to behave independently. We cannot ignore the possibility that

there is some level of contamination near the boundaries between the three subregions, but this contamination does not give rise to the systematic effects observed throughout the period displayed in Figure 1.

5.2. Juno Orbit 4

As suggested in the previous section, the global auroral morphology observed during the two- to three-week period around PJ04 (DOY 33.57) is different from PJ03. Figure 4 (and Figure S4.4) shows that for at least 16 days, the morphology was continuously influenced by injection signatures and/or characterized by a narrow dawnside ME. As a result, only the I, i, and N families are present. This strongly suggests that during that period, the inner-to-middle magnetosphere was probably adjusting to an enhanced logenic plasma production. This might have affected all auroral components, as shown in Figure 1 (and Figure S1.4), where the power in the three subregions evolved in parallel. The influence of the poleward subregion is more pronounced than in the case of PJ03, and the power values observed in it around PJ04 are among the largest ones of the present campaign. If one assumes that the contamination between the subregions is only marginal, this would mean that the internal plasma production has profound effects, not limited to the inner magnetosphere, but extending down the distant magnetosphere. Near perijove, the auroral morphology belonged to the i family and the total emitted power was around 1 TW, which is in the lower part of the range of power values measured around PJ04. Around the time of apojove of orbit 4 (DOY 59), two HST visits captured one i family member and two days later, a X family member. However, it should be noted that the emitted power is similar for both, suggesting that there is an uncertainty on the actual family of the X member, which may also fit the N family. Fortunately, this kind of ambiguity is relatively unusual and in most cases the power measured in the three subregions is in agreement with the selected morphological family.

5.3. Juno Orbit 5

The two-week period around perijove PJ05 (DOY 86.4) is characterized by auroral morphologies that evolved differently from orbits 3 and 4. In the case of orbit 5, about 10 days before perijove, the aurora showed signatures of magnetospheric compressions for almost three days (X family). It was then followed by a week of moderate injection signatures (i) that rapidly increased to strong injection signatures (I) just at the time of perijove PJ05. One day after, these equatorward subregion emissions decreased and gave way to four days of narrow dawnside ME (N family). The total emitted power shown in Figure 1 (and Figure S1.5) followed the same trend as in Figure 4 (and Figure S4.5), with values peaking above 2.4 TW, especially as a result of the enhanced equatorward-subregion emissions during the episodes of injection. The largest value, 2.6 TW, was reached when the morphology was in the X family and all three subregions were displaying large power values. Near perijove (I family), the total power reached 2.25 TW in the southern hemisphere and rapidly decreased (all subregions) to less than 2 TW in the northern hemisphere. Two HST visits were obtained near the time of apojove of orbit 5 (DOY 112). Both were characterized by extremely strong equatorward subregion emissions (I), giving rise to a total emitted power as large as 3.36 TW, which is the second highest power measured during the present HST campaign (the first highest, 3.52 TW, was during PJ06, as discussed below).

5.4. Juno Orbit 6

For 20 days around perijove PJ06 (DOY 139.28), HST observed a great deal of variability in the morphology. All families are well present, with the notable exception of X. For one week, the morphology seems to have "hesitated" between the Q and U families, both characterized by rather low and diffuse emissions (Figures 4 and S4.6). We estimate solar wind conditions upstream of Jupiter with the 1-D MHD model developed by Tao et al. (2005) and available from the online AMDA science analysis system. The accuracy of this propagation model largely depends on Earth-Sun-Jupiter angle, which we limited to about 20° in order to narrow down the uncertainty in the arrival times to less than 24 hr. The HST observations matching these limitations were mainly obtained during the approximately one-week period before the time of perijove PJ06. The weak and diffuse emissions (Q and U) that were observed at that time perfectly correlate with the continuously low solar wind dynamic pressure ($<$0.05 nPa) that persisted during that week, suggesting that the Q and U morphological families indeed correspond to episodes of low IM activity.

This low auroral period was interrupted by a short enhancement of the equatorward subregion (I) emission that was followed by two more quiet days (U). This temporary auroral enhancement occurred while the solar wind dynamic pressure was still below 0.05 nPa, suggesting that it was driven by processes taking place

inside the magnetosphere. Approaching the time of PJ06, the morphology grew more complex (N) and just after perijove, the southern hemisphere showed an extremely strong enhancement of the equatorward emission (I), about twice as much as what was observed during apojove 5. Again, this strong auroral event took place when the solar wind was relatively quiet. Contrary to other cases, the ME and poleward subregions did not follow the same dramatic increase and the total power "just" peaked around an extreme value of 3.52 TW **(**Figures 1 and S1.6**)**. This extreme event suggests that a major reconfiguration event might have taken place in the inner magnetosphere. During the days that followed, the auroral morphology gradually returned to a more undisturbed state (U and N). It is noteworthy that all along this period, the power emitted in the equatorward subregion was about twice the power in the poleward subregion, which itself was characterized by a power about twice that of the ME subregion. This clearly demonstrates how important it is not to restrict Jupiter's aurora to its main "oval," but to properly consider all the emissions equatorward and poleward of it. Near the time of apojove of orbit 6 (DOY 165), one HST visit captured a X family member for which the power distribution changed in comparison with the previous cases, since the ME surpassed the other subregions.

5.5. Juno Orbit 7

The 20 day period containing perijove PJ07 (DOY 192.11) is reminiscent of what was observed during orbit 6 (see above), at least for the week around perijove (Figures 4 and S4.7). After a three-day period of relatively quiet auroral activity (Q and U), the complexity of the morphology index increased to N and then to I in just a couple of days. A strong, localized injection occurred just at the time of PJ07. It was observed by HST in the southern hemisphere and resulted in a peak total power of 1.6 TW (Figures 1 and S1.7). The northern i family case that followed presents a similar total power since the loss of power in the equatorward subregion is almost entirely balanced by the 4 times larger emission power in the poleward subregion. During the week that followed PJ07, the auroral emission remained influenced by episodes of injection signatures interrupted by N family cases, and a second I family case took place on DOY 197 that reached 2.2 TW.

5.6. Connections Between the Families

The six morphological families that we identified in section 4 allow us to see how the auroral distribution is changing during different phases of the Juno mission. They also make it possible to determine how these typical morphologies relate to each other. Figure 5 shows the connections between all families. For example, the upper left "Q" panel describes how the Q family is connected with other ones. The red arrows, pointing to "Q," correspond to the transition(s) from the family observed during the visit directly preceding a Q case. The numbers next to the arrows indicate how many times such a transition was observed during the campaign between two adjacent visits separated by less than two days, amounting to 53 transitions. The number in parenthesis is limited to visits separated by less than a Jovian rotation. The blue arrows pointing away from "Q" correspond to direct transitions from a Q case to any other family. The numbers follow the same rule as for the red arrows. The next panels show the other transitions, such that all branches appear twice in the figure. Numbers in parentheses are significantly smaller since there are fewer visits separated by less than 1 Jovian rotation, amounting to 17 transitions, and for which we can assume that the overall morphology is not drastically changing in the interval. We note that in most cases they show the same trend as with the less-than-2-days numbers. Panel "Q" is dominated by U-Q and Q-U transitions. This is somewhat expected because both Q and U morphologies are very close, with Q being dimmer than U. These transitions thus correspond to a gradual change of the brightness of the auroral features contained in the ME subregion. Panel "N" reveals several transitions N-i, i-N, and N-I I-N, suggesting that the N family, characterized by a very narrow dawnside ME, is following or preceding episodes of plasma injections (I and i). Panel "I" then shows that there is probably a link between I and i families, which may show different stages of the evolution of the auroral signatures associated with plasma injections, although their characteristic time is usually less than one Jovian rotation. In panel "X", only one type of transition emerges: from X to i, suggesting that the X family, associated with IM compression, is often followed by plasma injections, implying that the disturbance caused by IM compression may trigger episodes of plasma injections in the middle magnetosphere, a scenario supported by Galileo particles and radio observations and reported by Louarn, Paranicas, and Kurth (2014). Interestingly, no typical family precedes an IM compression event, meaning that these events are indeed independent from the state of the

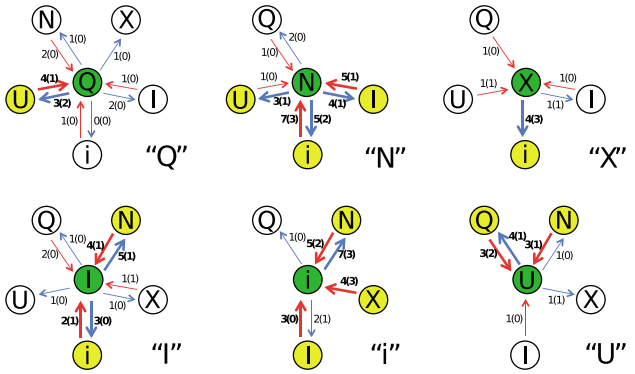

Figure 5. Graphical representation of the connections between all families. The upper left "Q" panel describes how the Q family (highlighted in green) is connected with other ones. The red arrows, pointing to Q, correspond to the transition(s) from the family observed during the HST visit directly preceding a Q case. The numbers next to the arrows indicate how many times such a transition was observed during the campaign between two adjacent HST visits separated by less than 2 days. The number in parenthesis is limited to visits separated by less than a Jovian rotation. The blue arrows pointing away from Q correspond to direct transitions from a Q family case to any other family. The numbers follow the same rule as for the red arrows. Cases where no transitions occur are not represented for clarity. The other panels show the other transitions, such that all branches appear twice in the figure. Numbers highlighted in bold and with thicker arrows correspond to the most likely transitions between families (highlighted in yellow).

magnetosphere, as expected for an external driver. Figure 5 also suggests that the N and i families could often change from one to the other. If these connections represent a systematic evolution, then it may challenge fundamental physics for which a nonadiabatic process cannot be reversible. Here we propose that the process from N family to i family is a natural evolution of the magnetospheric system involving processes like magnetic dipolarization, wave-particle interaction, and so on. This is contrary to the case of the i family to N family evolution, which would require an interruption of the system. Such an interruption may take place during the interaction between Jupiter's magnetosphere and the IM, for example, in the form of reconnection driven plasmoid release.

In parallel to Figure 5, a close inspection of Figure 4 suggests that episodes of plasma injection (I and i families) immediately following episodes of enhanced IM activity (X) are rather rare, with only four cases separated by less than a Jovian rotation (five cases if we extend this separation to two days). For the remaining 13 cases (48 if we count all cases separated by less than two days), these episodes appear disconnected, suggesting that the IM activity has a limited direct influence on the inner Jovian magnetosphere. On the contrary, the N family (narrow ME arc) almost systematically follows a period of injection (I and i families), which is compatible with the idea that during these periods of plasma injection, more plasma needs to be brought to corotation. Quiet periods (Q and U families) can last for as long as a week until they are interrupted by injection events. It is clear that the uneven temporal sampling of the aurora meant that we missed isolated events. Accordingly, there are probably gaps in the above scenarios.

Finally, it should be noted that the morphological evolution depicted in Figure 5 is only showing observed transition between two different families; it does not necessarily represent a physical or logical connection. Two families connected by an arrow could either suggest a natural evolution from one to the other, such as the development of plasma instability, or represent two irrelevant processes. For example, if we assume that family X is a consequence of IM compression, then it is possible to coincidentally have any other family prior to this family, as the appearance of IM compression is controlled by solar activity and obviously does not depend on the present condition of Jupiter.

6. Summary and Conclusions

In the present study, we report on observations of Jupiter's ultraviolet aurora with the STIS instrument onboard the HST during Juno orbits 3 to 7. The 118 selected STIS observations, or visits, of HST program GO-14634 are principally designed to complement Juno's remote-sensing instruments and to provide a longer monitoring of Jupiter's aurora, spanning a couple of weeks around each perijove, for Juno's in situ instruments. The morphology of Jupiter's aurora is known to be very complex and highly variable. It consists of several components, each of which represents a signature of physical processes taking place in different regions of the magnetosphere. As such, each image of Jupiter's aurora may be seen as an instantaneous snapshot of Jupiter's magnetospheric activity. However, the translation of variations of the auroral morphology to magnetospheric activity is far from obvious. One of the difficulties stems from the complexity of the aurora, especially in the northern hemisphere. In order to simplify things, we define three auroral subregions for each visit: ME, poleward, and equatorward, in which we measure the auroral emitted power as a function of time. We then define six auroral morphological families (Figure 3 and Table 2), representative of the morphologies that are typically observed during this campaign and which help us to quantify the morphological variations. Following previous similar auroral studies, we tentatively associate these families with magnetospheric activity.

1. The Q family is characterized by very low emission power of most auroral components, especially those filling the ME and equatorward subregions, and a rather large latitudinal extension. This morphology presumably corresponds to a quiet, undisturbed magnetosphere.
2. The N family also shows relatively low power, but with a very narrow dawnside ME arc. The rest of the ME also consists of relatively narrow arcs, together forming a relatively expanded ME. It very often follows a i family case and may correspond to a magnetosphere that returned to a quiet state after episodes of injections.
3. The U family is intermediate between the Q and N families, with relatively wide and faint dawnside ME, while the ME afternoon sector is usually brighter and narrower. It may then represent an intermediate stage in terms of magnetospheric configuration. The narrow and brightened auroral arc may be a signature of storage of large amounts of free energy, for example, in the form of plasma pressure gradient, stretched magnetic topology, or current sheet thinning. The magnetospheric configuration corresponding to the U family is likely to evolve in such a way as to release this energy through plasma instabilities like, for example, the development of interchange instabilities, which are potentially associated with plasma injections.
4. The I family is easily recognized by its strong enhancement of the equatorward emissions and the corner-shaped distribution near 150° S3 longitude in the north (70° in the south). These equatorward emissions are likely associated with injection of hot plasma resulting from an enhanced plasma transport from the Io torus. They often follow "quiet magnetosphere" Q and N family members.
5. The i family is similar to the I family but with significantly lower power, suggesting that the injected plasma is either in a more advanced stage of assimilation by the ambient plasma or in a developing stage.
6. The dawnside ME of the X family is very strong, and the afternoon side of the ME is also often bright and narrow. The dusk sector of the poleward subregion usually contains bright and highly variable auroral patches or arcs parallel to the ME. This family may result from an enhanced influence of the IM, such as the arrival of an IM compression region.

With the subregion power and morphological families, we show that the auroral and magnetospheric activities were different for each Juno orbit, from 3 to 7. This suggests that during these periods, internal factors (i.e., related to Io) and external factors (related to the IM) largely and unevenly influenced Jupiter's magnetosphere. The results presented here demonstrate that the auroral morphology is changing very rapidly, within one Jovian rotation, suggesting that the magnetosphere itself is rapidly adapting to the internal and external constraints. This study also demonstrates that it is imperative not to restrict Jupiter's aurora to its main "oval," but to address all the emissions both equatorward and poleward of it.

The two-week period around PJ03 was the most influenced by the IM, while during the two weeks around PJ04, HST only caught several episodes of plasma injection. The two-week period around PJ05 started with three days of high IM activity, followed by one week of moderate internal activity, and then by strong injections near perijove, followed by several days of N family aurorae. At the beginning, orbits 6 and 7 roughly follow similar trends, with one week of relatively quiet activity followed by strong injections near the time of perijove. The injection activity stops the day after in orbit 6 while it continues for several days at a moderate level in orbit 7. HST observations can be connected with the in situ and remote sensing of Juno in order to better establish the observational relationship between magnetospheric and auroral activity. In addition to our examination of the relationship of our results with the upstream solar wind, for PJ6, it will be helpful to determine whether any relationship can be established between increased Io activity or Io torus density for their potential influence on the evolution of auroral properties as noted between PJ03 and PJ07. This is possible with several ongoing studies of Io and the Io torus that are cross referenced with the work presented here in a full description of Juno-supporting observations that are summarized at a Web site maintained by the Juno mission: https://www.missionjuno.swri.edu/planned-observations. A more complete picture of the processes of energy transport associated with auroral phenomena and their evolution in time can be obtained by additional cross referencing of X-ray emission (e.g., Dunn et al., 2017), auroral emission from H_3^+ in the near infrared from the Jupiter Infrared Auroral Mapper among Juno's instrumentation (e.g., Mura et al., 2017), and supporting ground-based observations of H_3^+ emission (e.g., L. Moore, et al., 2017) and their associated influence on temperatures of Jupiter's upper stratosphere (e.g., Sinclair et al., 2017). The timing and scope of these observations are also summarized on the Juno-maintained Web site listed above.

Acknowledgments

B. B., D. G., Z. Y., B. P., and J. C. G. are supported by the PRODEX program managed by ESA in collaboration with the Belgian Federal Science Policy Office. A. R. was funded by the Fund for Scientific Research (F.R.S-FNRS). Z. Y. is funded by a Marie Curie COFUND post-doctoral fellowship. J. D. N. was supported by STFC grant ST/K001000/1. G. S. O. was supported by funds from the National Aeronautics and Space Administration distributed to the Jet Propulsion Laboratory, California Institute of Technology. The research at the University of Iowa was supported by NASA through contract 699041X with Southwest Research Institute. This research is based on observations with the NASA/ESA Hubble Space Telescope (program HST GO-14634), obtained at the Space Telescope Science Institute (STScI), which is operated by AURA for NASA. All data are publicly available at STScI. Solar wind parameters were propagated with the AMDA science analysis system provided by the Centre de Données de la Physique des Plasmas (CDPP) supported by CNRS, CNES, Observatoire de Paris, and Université Paul Sabatier, Toulouse. D. G. wishes to thank William Januszewski and John Debes, at STScI, for their invaluable help in programming the HST observations. We also wish to thank two anonymous reviewers for their very constructive comments and suggestions.

References

Badman, S. V., Bonfond, B., Fujimoto, M., Gray, R. L., Kasaba, Y., Kasahara, S., et al. (2016). Weakening of Jupiter's main auroral emission during January 2014. *Geophysical Research Letters*, *43*, 988–997. https://doi.org/10.1002/2015GL067366

Badman, S. V., Jackman, C. M., Nichols, J. D., Clarke, J. T., & Gérard, J.-C. (2014). Open flux in Saturn's magnetosphere. *Icarus*, *231*, 137–145. https://doi.org/10.1016/j.icarus.2013.12.004

Bagenal, F., Adriani, A., Allegrini, F., Bolton, S. J., Bonfond, B., Bunce, E. J., et al. (2014). Magnetospheric science objectives of the Juno mission. *Space Science Reviews*, *213*(1-4), 219–287. https://doi.org/10.1007/s11214-014-0036-8.

Bolton, S., Levin, S., & Bagenal, F. (2017). Juno's first glimpse of Jupiter's complexity. *Geophysical Research Letters*, *44*, 7663–7667. https://doi.org/10.1002/2017GL074118

Bonfond, B., Gladstone, G. R., Grodent, D., Greathouse, T. K., Versteeg, M. H., Hue, V., et al. (2017). Morphology of the UV aurorae Jupiter during Juno's first perijove observations. *Geophysical Research Letters*, *44*, 4463–4471. https://doi.org/10.1002/2017GL073114

Bonfond, B., Grodent, D., Badman, S. V., Gérard, J.-C., & Radioti, A. (2016). Dynamics of the flares in the active polar region of Jupiter. *Geophysical Research Letters*, *43*, 11,963–11,970. https://doi.org/10.1002/2016GL071757

Bonfond, B., Grodent, D., Badman, S., Saur, J., Gérard, J.-C., & Radioti, A. (2017). Similarity of the jovian satellite footprints: Spots multiplicity and dynamics. *Icarus*. https://doi.org/10.1016/j.icarus.2017.01.009, *292*, 208–217.

Bonfond, B., Grodent, D., Gérard, J.-C., Stallard, T., Clarke, J. T., Yoneda, M., et al. (2012). Auroral evidence of Io's control over the magnetosphere of Jupiter. *Geophysical Research Letters*, *39*, L01105. https://doi.org/10.1029/2011GL050253

Bonfond, B., Gustin, J., Gérard, J.-C., Grodent, D., Radioti, A., Palmaerts, B., et al. (2015). The far-ultraviolet main auroral emission at Jupiter – Part 1: Dawn–dusk brightness asymmetries. *Annales Geophysique*, *33*(10), 1203–1209. https://doi.org/10.5194/angeo-33-1203-2015

Bonfond, B., Vogt, M. F., Gérard, J.-C., Grodent, D., Radioti, A., & Coumans, V. (2011). Quasi-periodic polar flares at Jupiter: A signature of pulsed dayside reconnections? *Geophysical Research Letters*, *380*, L02104. https://doi.org/10.1029/2010GL045981

Chané, E., Saur, J., Keppens, R., & Poedts, S. (2017). How is the Jovian main auroral emission affected by the solar wind? *Journal of Geophysical Research: Space Physics*, *122*, 1960–1978. https://doi.org/10.1002/2016JA023318

Chané, E., Saur, J., & Poedts, S. (2013). Modeling Jupiter's magnetosphere: Influence of the internal sources. *Journal of Geophysical Research: Space Physics*, *118*, 2157–2172. https://doi.org/10.1002/jgra.50258

Clarke, J. T., Ballester, G., Trauger, J., Ajello, J., Pryor, W., Tobiska, K., et al. (1998). Hubble Space Telescope imaging of Jupiter's UV aurora during the Galileo orbiter mission. *Journal of Geophysical Research*, *103*(E9), 20,217–20,236. https://doi.org/10.1029/98JE01130

Connerney, J. E. P., Adriani, A., Allegrini, F., Bagenal, F., Bolton, S. J., Bonfond, B., et al. (2017). Jupiter's magnetosphere and aurorae observed by the Juno spacecraft during its first polar orbits. *Science*, *356*(6340), 826–832. https://doi.org/10.1126/science.aam5928

Cowley, S. W. H., & Bunce, E. J. (2001). Origin of the main auroral oval in Jupiter's coupled magnetosphere–ionosphere system. *Planetary and Space Science*, *49*(10-11), 1067–1088. https://doi.org/10.1016/S0032-0633(00)00167-7

Delamere, P. A., Bagenal, F., Paranicas, C., Masters, A., Radioti, A., Bonfond, B., et al. (2014). Solar wind and internally driven dynamics: Influences on magnetodiscs and auroral responses. *Space Science Reviews*, *187*(1-4), 51–97. https://doi.org/10.1007/s11214-014-0075-1

Delamere, P. A., Otto, A., Ma, X., Bagenal, F., & Wilson, R. J. (2015). Magnetic flux circulation in the rotationally driven giant magnetospheres. *Journal of Geophysical Research: Space Physics*, *120*, 4229–4245. https://doi.org/10.1002/2015JA021036

Dumont, M., Grodent, D., Radioti, A., Bonfond, B., & Gérard, J.-C. (2014). Jupiter's equatorward auroral features: Possible signatures of magnetospheric injections. *Journal of Geophysical Research: Space Physics*, *119*, 10,068–10,077. https://doi.org/10.1002/2014JA020527

Dunn, W. R., Branduardi-Raymont, G., Ray, L. C., Jackman, C. M., Kraft, R. P., Elsner, R. F., et al. (2017). The independent pulsations of Jupiter's northern and southern X-ray auroras. *Nature Astronomy*, *1*(11), 758–764. https://doi.org/10.1038/s41550-017-0262-6

Fear, R. C., Milan, S. E., Maggiolo, R., Fazakerley, A. N., Dandouras, I., & Mende, S. B. (2014). Direct observation of closed magnetic flux trapped in the high-latitude magnetosphere. *Science*, *346*(6216), 1506–1510. https://doi.org/10.1126/science.1257377

Gérard, J.-C., Bonfond, B., Grodent, D., & Radioti, A. (2016). The color ratio-intensity relation in the Jovian aurora: Hubble observations of auroral components. *Planetary and Space Science*, *131*, 14–23. https://doi.org/10.1016/j.pss.2016.06.004

Gérard, J.-C., Bonfond, B., Grodent, D., Radioti, A., Clarke, J. T., Gladstone, G. R., et al. (2014). Mapping the electron energy in Jupiter's aurora: Hubble spectral observations. *Journal of Geophysical Research: Space Physics*, *119*, 9072–9088. https://doi.org/10.1002/2014JA020514

Gérard, J. C., Grodent, D., Radioti, A., Bonfond, B., & Clarke, J. T. (2013). Hubble observations of Jupiter's north–south conjugate ultraviolet aurora. *Icarus*, *226*(2), 1559–1567. https://doi.org/10.1016/j.icarus.2013.08.017

Gladstone, G. R., Persyn, S. C., Eterno, J. S., Walther, B. C., Slater, D. C., Davis, M. W., et al. (2014). The ultraviolet spectrograph on NASA's Juno mission. *Space Science Reviews*, *213*(1-4), 447–473. https://doi.org/10.1007/s11214-014-0040-z

Gladstone, G. R., Versteeg, M. H., Greathouse, T. K., Hue, V., Davis, M. W., Gérard, J. C., et al. (2017). Juno-UVS approach observations of Jupiter's auroras. *Geophysical Research Letters*, *44*, 7668–7675. https://doi.org/10.1002/2017GL073377

Gray, R. L., Badman, S. V., Bonfond, B., Kimura, T., Misawa, H., Nichols, J. D., et al. (2016). Auroral evidence of radial transport at Jupiter during January 2014. *Journal of Geophysical Research: Space Physics*, *121*, 9972–9984. https://doi.org/10.1002/2016JA023007

Gray, R. L., Badman, S. V., Woodfield, E. E., & Tao, C. (2017). Characterization of Jupiter's secondary auroral oval and its response to hot plasma injections. *Journal of Geophysical Research: Space Physics*, *122*, 6415–6429. https://doi.org/10.1002/2017JA024214

Grodent, D. (2015). A brief review of ultraviolet auroral emissions on Giant planets. *Space Science Reviews*, *187*(1-4), 23–50. https://doi.org/10.1007/s11214-014-0052-8

Grodent, D., Bonfond, B., Gérard, J.-C., Radioti, A., Gustin, J., Clarke, J. T., et al. (2008). Auroral evidence of a localized magnetic anomaly in Jupiter's northern hemisphere. *Journal of Geophysical Research*, *113*, A09201. https://doi.org/10.1029/2008JA013185

Grodent, D., Clarke, J. T., Kim, J., Waite, J. H., & Cowley, S. W. H. (2003). Jupiter's main auroral oval observed with HST-STIS. *Journal of Geophysical Research*, *108*(A11), 1389. https://doi.org/10.1029/2003JA009921

Grodent, D., Clarke, J. T., Waite, J. H., Cowley, S. W. H., Gérard, J.-C., & Kim, J. (2003). Jupiter's polar auroral emissions. *Journal of Geophysical Research*, *108*(A10), 1366. https://doi.org/10.1029/2003JA010017

Grodent, D., Waite, J. H. Jr., & Gérard, J.-C. (2001). A self-consistent model of the Jovian auroral thermal structure. *Journal of Geophysical Research*, *106*(A7), 12,933–12,952. https://doi.org/10.1029/2000JA900129

Gustin, J., Bonfond, B., Grodent, D., & Gérard, J.-C. (2012). Conversion from HST ACS and STIS auroral counts into brightness, precipitated power, and radiated power for H2 giant planets. *Journal of Geophysical Research*, *117*, A07316. https://doi.org/10.1029/2012JA017607

Gustin, J., Cowley, S. W. H., Gérard, J.-C., Gladstone, G. R., Grodent, D., & Clarke, J. T. (2006). Characteristics of Jovian morning bright FUV aurora from Hubble Space Telescope/Space Telescope Imaging Spectrograph imaging and spectral observations. *Journal of Geophysical Research*, *111*, A09220. https://doi.org/10.1029/2006JA011730

Gustin, J., Grodent, D., Ray, L. C., Bonfond, B., Bunce, E. J., Nichols, J. D., & Ozak, N. (2016). Characteristics of north jovian aurora from STIS FUV spectral images. *Icarus*, *268*, 215–241. https://doi.org/10.1016/j.icarus.2015.12.048

Hill, T. W. (2001). The Jovian auroral oval. *Journal of Geophysical Research*, *106*(A5), 8101–8107. https://doi.org/10.1029/2000JA000302

Khurana, K. K., Kivelson, M. G., Vasyliunas, V. M., Krupp, N., Woch, J., Lagg, A., et al. (2004). The configuration of Jupiter's magnetosphere. In F. Bagenal, T. E. Dowling, & W. B. McKinnon (Eds.), *Jupiter. The Planet, Satellites and Magnetosphere* (pp. 593–616). Cambridge, UK: Cambridge University Press.

Kimura, T., Badman, S. V., Tao, C., Yoshioka, K., Murakami, G., Yamazaki, A., et al. (2015). Transient internally driven aurora at Jupiter discovered by Hisaki and the Hubble Space Telescope. *Geophysical Research Letters*, *42*, 1662–1668. https://doi.org/10.1002/2015GL063272

Kimura, T., Nichols, J. D., Gray, R. L., Tao, C., Murakami, G., Yamazaki, A., et al. (2017). Transient brightening of Jupiter's aurora observed by the Hisaki satellite and Hubble Space Telescope during approach phase of the Juno spacecraft. *Geophysical Research Letters*, *44*, 4523–4531. https://doi.org/10.1002/2017GL072912

Louarn, P., Paranicas, C. P., & Kurth, W. S. (2014). Global magnetodisk disturbances and energetic particle injections at Jupiter. *Journal of Geophysical Research: Space Physics*, *119*, 4495–4511. https://doi.org/10.1002/2014JA019846

Mauk, B. H., Haggerty, D. K., Paranicas, C., Clark, G., Kollmann, P., Rymer, A. M., et al. (2017). Discrete and broadband electron acceleration in Jupiter's powerful aurora. *Nature*, *549*(7670), 66–69. https://doi.org/10.1038/nature23648

Moore, K. M., Bloxham, J., Connerney, J. E. P., Jørgensen, J. L., & Merayo, J. M. G. (2017). The analysis of initial Juno magnetometer data using a sparse magnetic field representation. *Geophysical Research Letters*, *44*, 4687–4693. https://doi.org/10.1002/2017GL073133

Moore, L., O'Donoghue, J., Melin, H., Stallard, T., Tao, C., Zieger, B., et al. (2017). Variability of Jupiter's IR H3+ aurorae during Juno approach. *Geophysical Research Letters*, *44*, 4513–4522. https://doi.org/10.1002/2017GL073156

Mura, A., Adriani, A., Altieri, F., Connerney, J. E. P., Bolton, S. J., Moriconi, M. L., et al. (2017). Infrared observations of Jovian aurora from Juno's first orbits: Main oval and satellite foorprints. *Geophysical Research Letters*, *44*, 5308–5316. https://doi.org/10.1002/2017GL072954

Nichols, J. D., Badman, S. V., Bagenal, F., Bolton, S. J., Bonfond, B., Bunce, E. J., et al. (2017). Response of Jupiter's auroras to conditions in the interplanetary medium as measured by the Hubble Space Telescope and Juno. *Geophysical Research Letters*, *44*, 7643–7652. https://doi.org/10.1002/2017GL073029

Nichols, J. D., Bunce, E. J., Clarke, J. T., Cowley, S. W. H., Gérard, J.-C., Grodent, D., & Pryor, W. R. (2007). Response of Jupiter's UV auroras to interplanetary conditions as observed by the Hubble Space Telescope during the Cassini flyby campaign. *Journal of Geophysical Research*, *112*, A02203. https://doi.org/10.1029/2006JA012005

Nichols, J. D., Clarke, J. T., Gérard, J. C., & Grodent, D. (2009). Observations of Jovian polar auroral filaments. *Geophysical Research Letters*, *36*, L08101. https://doi.org/10.1029/2009GL037578

Nichols, J. D., Clarke, J. T., Gérard, J. C., Grodent, D., & Hansen, K. C. (2009). Variation of different components of Jupiter's auroral emission. *Journal of Geophysical Research*, *114*, A06210. https://doi.org/10.1029/2009JA014051

Nichols, J. D., Yeoman, T. K., Bunce, E. J., Chowdhury, M. N., Cowley, S. W. H., & Robinson, T. R. (2017). Periodic emission within Jupiter's main auroral oval. *Geophysical Research Letters*, *44*, 9192–9198. https://doi.org/10.1002/2017GL074824

Palmaerts, B., Radioti, A., Grodent, D., Chané, E., & Bonfond, B. (2014). Transient small-scale structure in the main auroral emission at Jupiter. *Journal of Geophysical Research: Space Physics*, *119*, 9931–9938. https://doi.org/10.1002/2014JA020688

Radioti, A., Gérard, J.-C., Grodent, D., Bonfond, B., Krupp, N., & Woch, J. (2008). Discontinuity in Jupiter's main auroral oval. *Journal of Geophysical Research*, *113*, A01215. https://doi.org/10.1029/2007JA012610

Radioti, A., Tomas, A. T., Grodent, D., Gérard, J.-C., Gustin, J., Bonfond, B., et al. (2009). Equatorward diffuse auroral emissions at Jupiter: Simultaneous HST and Galileo observations. *Geophysical Research Letters*, *36*, L07101. https://doi.org/10.1029/2009GL037857

Sinclair, J. A., Orton, G. S., Greathouse, T. K., Fletcher, L. N., Tao, C., Gladstone, G. R., et al. (2017). Independent evolution of stratospheric temperatures in Jupiter's northern and southern auroral regions from 2014 to 2016. *Geophysical Research Letters*, *44*, 5345–5354. https://doi.org/10.1002/2017GL073529

Tao, C., Kataoka, R., Fukunishi, H., Takahashi, Y., & Yokoyama, T. (2005). Magnetic field variations in the Jovian magnetotail induced by solar wind dynamic pressure enhancements. *Journal of Geophysical Research*, *110*, A11208. https://doi.org/10.1029/2004JA010959

Vogt, M. F., Bunce, E. J., Kivelson, M. G., Khurana, K. K., Walker, R. J., Radioti, A., et al. (2015). Magnetosphere-ionosphere mapping at Jupiter: Quantifying the effects of using different internal field models. *Journal of Geophysical Research: Space Physics*, *120*, 2584–2599. https://doi.org/10.1002/2014JA020729

Yao, Z. H., Coates, A. J., Ray, L. C., Rae, I. J., Grodent, D., Jones, G. H., et al. (2017). Corotating magnetic reconnection site in Saturn's magnetosphere. *Astrophysical Journal Letters*, *846*(2), 7. https://doi.org/10.3847/2041-8213/aa88af

Yoshikawa, I., Suzuki, F., Hikida, R., Yoshioka, K., Murakami, G., Tsuchiya, F., et al. (2017). Volcanic activity on Io and its influence on the dynamics of the Jovian magnetosphere observed by EXCEED/Hisaki in 2015. *Earth, Planets and Space*, *69*(1), 110. https://doi.org/10.1186/s40623-017-0700-9